Single-cell protein analysis reveals metastable states during the transition to a sensory organ fate

Ritika Giri[1,2], Shannon Brady[1], and Richard W. Carthew[1,2,3]*

1. Department of Molecular Biosciences, Northwestern University, Evanston IL 60208

2. NSF-Simons Center for Quantitative Biology, Northwestern University, Evanston IL 60208

3. Lead Contact

* Correspondence: r-carthew@northwestern.edu

Keywords: Drosophila, Senseless, sensory neuron development

Abstract

Cell fate decisions can be envisioned as bifurcating dynamical systems, and the decision that *Drosophila* cells make to undergo sensory organ differentiation has been sucessfully described as such. We have extended these studies by focusing on the Senseless protein, which orchestrates the sensory fate transition. Wing cells contain intermediate Senseless numbers prior to their fate transition, after which they express much greater numbers of Senseless molecules as they differentiate. However, the dynamics are not consistent with it being a simple bistable system. Cells with intermediate Senseless are best modeled as residing in four discrete states, each with a distinct protein number and occupying a specific region of the tissue. Although the four states are stable over time, the number of molecules in each state vary with time. Remarkably, the fold-change in molecule number between adjacent states is invariant and robust to absolute protein number variation. Thus, cells transitioning to sensory fates exhibit metastability with relativistic properties.

Introduction

Animal development requires the progressive restriction of cells into distinct fate lineages. Before reaching their terminal fate, most cells transition through a number of stable lineage states, such that the fate potential of a cell is progressively restricted with each transition. C.H. Waddington famously compared the path that a cell takes towards its ultimate fate to a ball rolling down a contoured landscape and coming to rest at a terminal (Waddington, 1957).

Attractor states have long been proposed to represent distinct stable cell states, with transitions between attractor states being modeled as bifurcation events (Corson and Siggia, 2012; Huang et al., 2005). Waddington's landscape imagines there to be pitchfork bifurcations, where one state bifurcates into two stable states. With such bifurcations, the dynamical system is initially in a single stable steady state. Beyond the bifurcation, the original state remains a steady state but becomes unstable. Two new stable steady states appear, and these are symmetrical. In spite of the graphical similarity between Waddington's metaphor and pitchfork bifurcations in dynamical systems (Marco et al., 2014), there are other means by which cells could make fate choices over time. Saddle-node or fold bifurcations create new stable steady states somewhere distant from the initial steady state, which ceases to exist by dead ending. Unlike pitchfork bifurcations, the initial steady state is always unstable and is intermediate between the two stable states. Therefore, a dynamical system does not remain for a significant amount of time in this intermediate state but rapidly moves into a new stable state.

It is non-trivial to distinguish whether cell fate transitions should be modeled as pitchfork or saddle-node bifurcations (Freedman et al., 2021). Both could be invoked to explain the behavior of molecular determinants of cell fates (Marco et al., 2014; Rand et al., 2021). Fate transitions often involve the intermediate expression of a molecular determinant, which is then interpreted in a dichotomous manner by individual cells, to adopt divergent fates (Levine et al., 2013). For example, mouse neural progenitor

cells co-express fluctuating levels of three transcription factors, Ascl1/Mash1, Hes1 and Olig2, which promote fate choices to become neurons, astrocytes, and oligodendrocytes, respectively (Imayoshi et al., 2013). Subsequently, each differentiated lineage is characterized by high sustained expression of only one of the factors.

A different example is seen in developing structures that give rise to the adult *Drosophila* body. Sensory bristles on the adult epidermis derive from cells called sensory organ precursors (SOPs). Each SOP cell emerges from a group of cells expressing intermediate levels of proneural transcription factors from the *Achaete-Scute* (*Ac-Sc*) gene complex and the *senseless* (*sens*) gene (Garcia-Bellido and de Celis, 2009; Jafar-Nejad et al., 2003; Jafar-Nejad et al., 2006). The SOP is selected from the group by the action of Notch-mediated lateral inhibition, leading to sustained high expression of Sens and Ac-Sc proteins by a positive feedback mechanism (Nolo et al., 2000, 2001). In contrast, cells not selected for SOP fate downregulate Sens and Ac-Sc expression, and become epidermal cells. Mathematical modeling of the system as a saddle-node bifurcation has successfully described these dynamics, according to which an initial unstable state of intermediate proneural gene expression resolves into two stable states with high and low proneural expression (Corson et al., 2017).

When considering cell fate transitions as described above, it is generally assumed that the initial steady state has a fixed average expression level of fate determinants, with noise creating continuous variation in levels between cells. However, mammalian pluripotent embryonic stem (ES) cells can express fate determinants heterogeneously such that they resemble discrete states of expression. It is thought that ES cells can reversibly transit between these discrete states, thereby becoming temporarily biased to adopt specific differentiated fates (Klein et al., 2015). These states have been termed metastable, akin to the definition in physics of an energy state with a longer lifetime than that generated by random fluctuation but with a shorter lifetime than the ground state. From a dynamical perspective, the definition of metastability varies according to the approaches dealing with the issue (Kelso, 2012).

For example, metastability has been described as a system that explores its state space on different time scales. On fast time scales, transitions happen within a single subregion of state space, and on slow time scales they occur between different subregions. Metastability has also been described as a regime near a saddle-node bifurcation in which stable and unstable states no longer exist but attraction remains to where those fixed points used to be. However, it is unclear if metastable cell states are a general feature of developmental fate transitions.

Results

Sens is necessary for selection of SOP cells and development of sensory organs across the adult *Drosophila* body. We chose to focus on development of chemosensory organs located at the anterior margin of the adult wing (Fig. 1A). The wing develops from an elliptically shaped columnar epithelium known as the wing pouch, which grows in size during the larval life stages (Fig. 1B). SOP cells that give rise to the chemosensory organs first appear at the transition between the larval and pupal stages of life. The SOPs develop in two periodic rows flanking the midline that bisects the dorsal and ventral halves of the wing pouch (Fig. 1C). This can be microscopically visualized by measuring Sens protein abundance in cells (Fig. 1D). Some time later, each SOP divides twice, and the four descendents differentiate into a single sensory organ.

Sens expression is first detected during the larval stage prior to detection of the SOP cells (Fig. 1E). It is initially expressed at low levels within two stripes that are 3 - 6 cells in width and flank the dorsal-ventral midline. Expression is induced by the Wnt signaling protein Wingless (Wg), which is secreted by midline cells and whose expression increases over time (Fig. 1F,H) (Jafar-Nejad et al., 2006; Zecca et al., 1996). A subset of Sens-positive cells then dramatically increase Sens expression and become SOPs (Fig. 1G,H); these are typically located in the center of each stripe. This selection process is mediated by Delta-Notch mediated lateral inhibition (Hinz et al., 1994). Cells expressing higher levels of Sens express Delta ligand more strongly (Nolo et al., 2001). This leads to stronger Notch receptor

activation in neighbors, resulting in inhibition of Sens expression and down-regulation of Delta in the neighbors (Jafar-Nejad et al., 2003). These neighbors are then less effective at inhibiting Sens in the stronger expressing cell, leading to even stronger expression. Since Sens protein can activate *Ac-Sc* expression and its own expression (Acar et al., 2006; Jafar-Nejad et al., 2003; Nolo et al., 2000), the Delta-Notch lateral inhibitory process is further amplified. Thus, small initial differences in the levels of Sens protein between neighboring cells evolve into large differences (Fig. S1A,B). The system is thought to have bistability, such that intermediate levels of Sens are unstable, and cells transit to either high Sens (SOPs) or low Sens (epidermal) stable states (Fig. S1C).

Recently, an elegant mathematical model was formulated to describe SOP pattern formation of the dorsal thorax (Corson et al., 2017). We adapted this model to mimic development of the wing margin SOPs, in order to predict the dynamics of Sens expression. The model variable u describes the proneural activity in each cell, while variable s describes the inhibitory activity of Delta being received by each cell. The model takes the form

$$\tau\, du/dt = f(u-s) - u + \eta(t)$$

where τ is a scaling factor for time t, and η is Brownian noise. Although the variable u is not formally the level of an individual proneural factor like Sens, the model allows for the variable to approximate it. To simulate patterning of the wing margin, we prescribed the system as a single row of cells in which the Sens level u evolves over time, and resolves into an epidermal state (u = 0) or SOP state (u = 1). All simulation parameters are described explicitly in the Methods.

For all cells, u first reaches an intermediate steady state that lasts for some variable amount of time until u bifurcates towards the 0 or 1 final states. This transient steady state represents an unstable one, since the system has a saddle-node bifurcation (Fig. 2A). In model simulations, the time course of cell state shows a gradual progression of cells toward the SOP state, accompanied by

a continuous branching off of cells that relax to zero u (Fig. 2B). The final pattern of cell states resembles that observed for the wing margin SOPs; a row of periodically spaced SOPs (Fig. 2C). Although these model simulations predict Sens dynamics that could be tested in live wing pouch tissue, conditions to culture wing pouches *ex vivo* and maintain their intact development are not yet achievable (Handke et al., 2014; Zartman et al., 2013). Thus we could not directly observe Sens dynamics by live imaging.

To make a prediction from the model that we could experimentally test, the distributions of cells with different values of u were captured at different time points in simulations. At early time points in the model simulations, a unimodal distribution of cells rapidly shifts toward higher levels of u (Fig. 2D). At the unstable steady state (arrow), the distribution stabilizes but begins to skew downwards until it forms a clear bimodal distribution, with some cells shifting upward and other cells rapidly shifting downward (Fig. 2D). This provided us with a testable prediction of the model since we could quantitatively measure Sens protein in many single cells from wing pouches fixed at different time points during SOP determination.

A mixture model describes Sens protein distribution

To measure Sens protein levels in single cells, we employed a genomic *sens* transgene tagged at the N-terminus with sfGFP (Fig. S2). The transgene fully recapitulates the endogenous *sens gene* expression pattern, and fully rescues the developmental defects of *sens* mutant alleles (Giri et al., 2020). All experiments were performed with two copies of the transgene in a *sens* mutant background.

Single-cell Sens levels were quantified using a previously described automated image analysis pipeline (Giri et al., 2020). Wing pouches from transgenic animals were fixed and imaged with a confocal microscope. Single cells were identified by computational image segmentation, and Sens was quantified as the average sfGFP fluorescence signal in each segmented cell. Relative fluorescence

signals were converted to absolute sfGFP-Sens molecule numbers using a calibration factor that was empirically determined by Fluorescence Correlation Spectroscopy (Giri et al., 2020). For each experimental condition in our study, between 6,000 and 12,000 Sens-positive cells were segmented and analyzed.

Wing pouches were dissected from late third instar larvae ~ 1 - 2 hours before SOPs are first detected. Several wing pouches were subjected to the automated analysis pipeline and pooled to generate a high-resolution expression profile for Sens (Fig. 3A). Sens-positive cells displayed a wide range of protein numbers. However, 90% of cells expressed fewer than 2,000 molecules per cell, and the majority of those contained fewer than 200 molecules per cell. We then dissected wing pouches from animals undergoing the larval-pupal transition, when the first SOPs have formed. There was a near two-fold increase in Sens numbers per cell relative to the earlier time-point (Fig. 3B). The median number of 188 molecules per cell in larval cells shifted to 374 molecules per cell in the larval-pupal cells. The difference in Sens numbers over time was statistically significant and corresponded to an increase of 186 molecules (95% confidence interval 175-197 molecules). Since SOP cells were visibly apparent at the larval-pupal transition, we counted Sens protein number in these cells and found them to contain from 1,500 to over 10,000 molecules per cell.

We focused our analysis on cells with intermediate Sens levels since these cells were predicted to be approaching the unstable steady state. Within these cells, there appeared to be a multimodal distribution of Sens protein number, with a single major peak and a number of smaller peaks with higher Sens number (Figs. 3C and S3). In order to rigorously assess the composition of the Sens-positive cell population, Sens distributions obtained from individual wing pouches were subjected to mixture model analysis. A mixture model is a probabilistic model that predicts the number of discrete states present in an overall set of observations, without mapping individual data points to a specific state. We fit a Gaussian mixture model to the Sens expression data. Model quality was determined by calculating the

Akaike Information Criterion (AIC) and Bayesian Information Criterion (BIC) scores for models with different numbers of states (Claeskens and Hjort, 2008). A model with four discrete states was repeatedly found to best-fit the distributions observed in replicate wing pouches from both the larval and larval-pupal stages (Fig. 3D, Fig S4). This analysis suggests that cells expressing intermediate levels of Sens do not show a simple pattern of variation around a single mean, as predicted by the dynamical model (Fig. 2D), but rather there is unanticipated heterogeneity in their expression.

Each cell state in the Gaussian mixture model is defined by three parameters: the mean Sens protein number, the standard deviation around the mean, and the fractional representation of the state in the total cell population. For instance, a cell state with a mean expression of 100 molecules, standard deviation of 20 molecules, and fractional proportion of 0.3 would indicate that 30% of all Sens-positive cells are in a state centered at 100 ±20 Sens molecules. We labelled the different Sens states from 1 to 4, with state 1 having the lowest number of Sens molecules per cell and state 4 having the highest (Table 1). For both the early and late stages, there appeared to be a non-linear increase in average Sens number when comparing one state to the next (Fig. 3E). When comparing early and late developmental stages, the average Sens number differed by two-fold between states with the same label (Fig. 3E). However it is important to note that the similar labeling of states at different stages does not necessarily imply that they are the same. Cells labeled state 1 at the early stage are not necessarily in the same internal state as cells labeled state 1 at the late stage.

We converted the fractional proportion of cells in a given state to the absolute number of cells in that state. Conversion was performed in order to compare stages, since the total number of Sens-positive cells in the imaged regions increased from 198 ±41 in larval wing pouches to 279 ± 21 in in larval-pupal pouches. At the larval stage, the imaged region in the pouch contained approximately 50 cells in each of the four states (Fig. 3F). At the later larval-pupal stage, there remained 50 cells in state 1, but there were more cells in states 2 and 3, while fewer cells were found to be in state 4 (Fig. 3F).

This observation did not fit with expectations of the dynamical model, where as time proceeds, cells bifurcate towards low and high states (Fig. 2D). If that were true, we would have observed more cells in the lowest and highest states of 1 and 4. Instead, more cells were detected in the two intermediate states 2 and 3.

Cells in different states occupy overlapping regions in the wing pouch

Wg molecules activate *sens* transcription on either side of the dorsal-ventral midline up to eight cell diameters away (Eivers et al., 2009; Giri et al., 2020). Since Wg concentration decays with distance from the midline (Alexandre et al., 2014), it is possible that cells at different distances receive different doses of the activating signal. If Sens expression is proportional to the signal dose, then the resulting distribution would resemble an *n*-state mixture, where *n* distinct doses of Wg are interpreted as *n* cell states.

Therefore, we examined the relationship between the distance of a cell from the Wg source, and its Sens expression level. The midline was manually delineated, and the shortest Euclidean distance from each cell centroid to the midline was calculated (Fig. S5). As expected, Sens-positive cells were located no further than eight cell-diameters from the midline. However, Sens protein numbers were weakly correlated with distance, with correlation coefficients ranging from 0.25 to 0.35 for individual samples (Fig. 4A). At both early and late stages, cells close to the midline displayed a wide range of Sens protein number. As distance from the midline increased, the range of Sens number narrowed, and cells expressed fewer Sens molecules.

To ascertain where cells in a given state are located, we classified cells according to their likely state. This was done by assigning cells with Sens levels within one standard deviation from the mean value of a given state. Each cell's distance from the midline was then calculated as before. At the larval stage, cells had a nested spatial distribution with respect to distance from the midline (Fig. 4B). Cells in state 1 were distributed over the greatest distance, followed by cells in state 2, state 3 and state 4,

each with progressively more restricted spatial distributions. In a zone located 5 to 15 μm from the midline, cells in all four states coexisted (Fig. 4B). At the larval-pupal transition, the nested spatial distribution of states was also observed (Fig. 4C). However, the distributions were narrower; the distal boundaries of cells in states 1 and 2 were much closer to the midline. The proximal boundary of cells in state 4 was more distant from the midline, and the distal boundary also appeared to have shifted. When we mapped visible SOPs to these distributions, the SOPs were located in the central zone in which cells in all four states resided. The nested distribution of states suggests that Wg dose alone does not determine Sens state.

The spatial position of cells in various states was conserved between larval and larval-pupal stages (Fig. 4D). There was large overlap in position between cells labelled state 1 at the early stage and cells labelled state 1 at the late stage, and so on. Cells in the wing pouch do not move relative to one another at this period of wing development. Hence, the results suggest that individual states are maintained over time, i.e. cells labelled state 4 at the early stage are probably in the same internal state as those labelled state 4 at the later stage. If a given state is maintained over time, this would suggest that between the early and late stages, some cells transitioned between states. The reason for this supposition is that some regions with cells in a given state at the early stage no longer had such cells later (Fig. 4D). For example, state 1 cells very distal from the midline at the larval stage likely became Sens-negative by the pupal transition. State 2 cells distal from the midline at the larval stage either became Sens-negative or transitioned to state 1. The overall implication is that while internal states are maintained over time, some cells transition into or out of particular states over time.

States are robust to perturbation of absolute Sens number

If internal states are maintained over time, they are nevertheless dynamic in terms of Sens molecule number. There is a two-fold increase in Sens number within cells of a given state from early to late stages. There is also a change in the number of cells in a given state over time. It is therefore possible

that an increase in Sens number alters the likelihood that cells remain in a particular state. To test the idea, Sens expression was genetically perturbed, and the resulting distribution was analyzed to determine cell-state properties. Sens expression was perturbed by ablating miR-9a regulation of *sens*. MicroRNAs are non-coding RNA molecules that bind to target mRNAs in a sequence-specific manner and modestly repress protein output (Carthew and Sontheimer, 2009). We and others had shown that miR-9a inhibits Sens protein output by binding to two sites in the *sens* mRNA 3'UTR (Cassidy et al., 2013; Giri et al., 2020; Li et al., 2006). To test the effect of miR-9a regulation on cell state properties, the miR-9a binding sites in the *sens* transgene were combinatorially mutated to generate a series of *sens* alleles. Alleles were landed in the same genomic location as the wild-type *sens* transgene. All transgenes rescued *sens* mutant phenotypes and recapitulated the endogenous *sens* expression pattern (Fig. S6A).

The single binding site mutants *sens-m1* and *sens-m2* displayed only modest changes in Sens expression (Fig. S6B). When both binding sites were mutated in *sens-m1m2*, there was a significant increase in Sens expression (Figs. 5A and S6C). This indicates that the two binding sites are functionally redundant *in vivo*, such that a single site can confer near-complete repression. With loss of both binding sites, median single-cell Sens levels increased from 374 molecules to 616 molecules per cell, a 1.65-fold increase (Fig. 5A). Increased expression was a direct consequence of loss of miR-9a binding, since the expression profiles did not significantly differ in a *mir-9a* mutant background (Fig. S6D).

Cell populations from the *sens-m1m2* wing pouches were then subject to mixture model analysis. Again, four states were determined to be the best-fit model for the mutant expression profile. The average Sens molecule number in each state was uniformly higher when miR-9a regulation was ablated, suggesting that miR-9a regulates expression in a state-independent manner (Fig. 5B). Importantly, there was little effect of the *sens-m1m2* mutant on the number of cells in each state at both

larval and larval-pupal stages (Fig. 5C,D). These results suggest that the cell states are robust against loss of miR-9a regulation of protein output. Hence, the developmental change in cell-state population size seen in wildtype is not simply due to the increase in Sens protein number over that time period. If it had been, then cell-state population sizes would have differed between the wildtype and *sens* mutant at the same developmental stage, which was not observed.

To further test the insensitivity of cell states to absolute Sens numbers, we raised animals at different temperatures. The previous experiments had all been conducted at a room temperature of 22 - 24°C. Two other temperatures, 18°C and 29°C, were chosen to assess cell state properties at the larval-pupal transition. At both 18°C and 29°C, the Sens expression pattern appeared normal (Fig. S7A). However, median Sens number was two-fold higher when growth temperature was increased from 18°C to 29°C (Fig. 5E).

Sens-positive cell populations from 18°C and 29°C were subjected to mixed model analysis to determine if cell state characteristics were altered. Again, a mixed model with four states was the best-fit whether at 18 or 29°C. The average Sens levels uniformly increased for all four states from 18°C to 29°C (Fig. 5F). However, no significant difference was observed in cell-state population size between the two temperatures (Fig. 5G). As a final test, animals with different *sens* alleles were subjected to temperature variation. Compared to wildtype *sens* animals raised at 18°C, *sens-m1m2* animals raised at 29°C showed a four-fold increase in average Sens protein number for all states (Fig. S7B). However, there was little change in cell-state population size (Fig. S7C). Altogether, these results indicate that the relative number of cells in each state is robust against variation in Sens number.

States differ by a fixed ratio of Sens protein numbers per cell

We next analyzed the relative levels of Sens in states by calculating the ratio of average Sens molecule number between adjacent states. The ratios of Sens in state 2 vs state 1, state 3 vs state 2, and state 4 vs state 3 were strikingly similar to one another (Fig. 6A). Ratio values ranged from 2.6 to

2.8, in spite of the large differences in Sens protein number between the states. Remarkably, these ratios were invariant when measured in cells at the larval stage, at the larval-pupal stage, at 18°C, and when miR-9a regulation of *sens* was nullified (Fig. 6A). The ratios were slightly higher (~ 3.1) when animals were grown at 29°C (p = 0.0002, t-test), but nonetheless were still invariant between neighboring states (Fig. 6A). This result indicates that the proneural system elicits fold-changes in Sens number when cells transition to particular states. If this interpretation is correct, then states are not determined so much by an absolute number of Sens molecules as by a relative number.

Discussion

A simple saddle-node bifurcation model of SOP selection at the wing margin predicts that before the bifurcation, Sens levels become unimodally distributed around an intermediate unstable steady state. Once selected, the model predicts SOP-fated precursors continuously increase Sens to its maximal value, while epidermal-fated precursors continuously reduce Sens to its minimal value. However, single-cell protein quantitation during development *in vivo* reveals an unanticipated distribution of cells into four discrete subpopulations expressing low-to-intermediate levels of Sens. These subpopulations are maintained in the face of differences in developmental stage, growth temperature, and miR-9a regulation, indicating that the four-state distribution is a stable property of Sens expression in proneural cells of the wing margin.

The existence of stable subpopulations suggests the system has metastability. There are two distinct ways in which the system could create this metastability. One, cells could begin to express Sens and then continuously increase Sens number until cells reach any one of the four possible states (Fig. 6B). The likelihood a cell adopts a particular state might depend on variables such as its distance from the midline. However, once a cell adopts that particular state, it does not transition to one of the other three states, but it either relaxes to being Sens-negative or it transitions to the SOP fate. The likelihood a cell in a particular state can become an SOP might vary with its state identity, i.e. have

zero likelihood if it is in state 1, 2, and 3 but some positive likelihood if it is in state 4. This scenario would be consistent with the fact that all SOPs emerge only in the narrow zone where cells in state 4 reside.

A second way in which the system could have metastability would be that cells can transition between different metastable states with some probability dependent on a variable such as distance from the midline (Fig. 6C). For example, a cell in state 1 could transition to state 2 and vice versa. Transitions could conceivably be limited to adjacent states or might include switches to non-adjacent states, i.e. state 1 to state 3. If the system operates this way, then the transition of a competent proneural cell to its SOP fate is not a continuous process, but requires multiple transitions between metastable states before the SOP fate is adopted. Such metastable systems have been observed in other developmental contexts, and have been shown to have functional roles (Antolovic et al., 2019; Chang et al., 2008; Klein et al., 2015; Olsson et al., 2016).

This raises the question as to what gives rise to these discrete states? One possibility is that burst-like transcription of genes generates discrete pulses of protein number that accumulate over time. Transcription initiation is rarely a continuous process for genes, even those that are constitutive. Short periods of time in which multiple transcripts are initiated are interspersed by periods of time in which no initiation occurs. If the average timescale between bursts is long enough, then discrete bursts of mRNA number lead to multimodality in protein number (Thomas et al., 2014). Indeed, modeling of *sens* transcription in the wing margin suggests that in lowly expressing cells, timescales of the on and off periods are approximately equivalent (Bakker et al., 2020; Giri et al., 2020). These studies also indicate that an average of four *sens* mRNAs are generated per burst, and each mRNA is translated on average into ten Sens protein molecules (Giri et al., 2020). Thus, a single burst would result in the average accumulation of ~ 40 Sens protein molecules. Moreover, burst size remains constant in cells experiencing different levels of Sens expression (Bakker et al., 2020). Since the average Sens protein

number in state 1 cells at the larval stage is 56 and at the larval-pupal stage is 109, it is plausible that state 1 represents cells after one or two transcriptional bursts of *sens*. State 2 could also conceivably be created by bursting kinetics. The average Sens number in state 2 cells at the larval stage is 115 and at the larval-pupal stage is 270, which would correspond to two and five transcription bursts, respectively.

However, a model in which transcription bursts generate discretization of all four states has a number of problems. The 40 molecule burst size is much smaller than the average number of Sens molecules at the larval stage for states 3 and 4. These numbers increase to 710 and 1,760 molecules for states 3 and 4 respectively, at the larval-pupal transition. One would estimate then that between 10 and 24 bursts of *sens* transcription occurred in cells within states 3 and 4 over the 1 - 2 hour period between stages. Thus, increments in bursting do not obviously translate to increments in protein number for states 3 and 4. Another problem with the burst model is the invariant ratio of Sens number observed within cells in adjacent states. It is difficult to reconcile how incremental bursting would translate to a relativistic difference in protein output.

An alternate mechanism is that the Wg and Delta signals are transduced into discrete *sens* activation states. While the states do not spatially correlate with the known concentration gradient of Wg, it is possible that the states are related to a combination of signals. If so, the distribution of the Notch ligand Delta would be an ideal candidate. Gradients of Delta have been proposed to drive sensory fate resolution in the thorax (Corson et al., 2017). Cells located in the center of thoracic stripes of proneural expression receive less Delta inhibition and therefore keep progressing to SOP fates while more lateral cells are robustly inhibited. However, there is no evidence of gradients of Delta expression in wing margin cells that resemble the thoracic stripes (Kooh et al., 1993). A more likely distribution of Delta might be that it is also discrete, since Delta is transcriptionally activated by Sens in wing margin cells (Nolo et al., 2001). Thus, cells in one Sens state would express Delta at a level that reflects a

discrete state of expression different from cells in other Sens states. In turn, such Delta discretization would feedback and enhance the discretization of Sens expression. It will be interesting to determine if multimodal expression of Delta exists in wing margin cells and how their states relate to the Sens states.

Another explanation for Sens metastability might be related to the dynamics of Wg synthesis and secretion. If transcription-translation of Wg occurs in bursts, then it is possible that midline cells secrete Wg in a pulsatile manner. Nearby cells would receive and transduce the Wg signal with pulsatile dynamics, resulting in discrete time periods when transcription-translation of Sens would occur. Of course, the correct mechanism might be some combination of these various models.

Intriguingly, the metastable states have properties that are relativistic with one another. The ratio of Sens number between adjacent states is invariant across a wide range of absolute Sens protein number. And the number of Sens-positive cells in a particular state is also invariant over a wide range of Sens protein number. These relativistic properties might provide robustness against variation in absolute expression due to genetic and environmental perturbations. Relativistic properties have not been observed in developmental systems exhibiting evidence of metastability. There is precedent for Wnt ligands inducing a fold-change in signal transduction to the nucleus rather than a change in absolute level (Goentoro and Kirschner, 2009). A similar feature has also been described for other signals, where target genes of the pathways respond to fold-change in signal transduction (Frick et al., 2017; Lee et al., 2014). If metastability of Sens is controlled by Wg and Delta signaling, one possibility is that fold-change in signal transduction over time is translated into relativistic maintenance of the four metastable states.

Our study raises many questions that remain unanswered. What is the nature of the metastability and what causes it? Why is it relativistic? And are the different states disposed to adopting particular terminal fates with different probabilities? These questions will be more robustly addressed once an ex vivo live imaging system of the late larval wing pouch becomes available.

Methods

Fly strains and genetics

All stocks were obtained from the Bloomington Drosophila Stock Center (BDSC) unless stated otherwise. Wild-type refers to stock w^{1118}. MicroRNA miR-9a null mutant stocks $mir9a^{E39}$ and $mir9a^{J22}$ were provided courtesy of the Gao Lab (Li et al., 2006). The *sens* mutant alleles used $sens^{E1}$ and $sens^{E2}$ are protein null mutants (Nolo et al., 2000, 2001).

Generation of *sens* transgenic stocks

The *sfGFP-sens* P[acman] transgenic construct, tagged with a N-terminal 3xFlag-TEV-StrepII-sfGFP-FlAsH, was originally generated from the CH322-01N16 BAC and is a kind gift from K. Venken and H. Bellen (Venken et al., 2006). The *miR-9a* binding site mutant alleles of the *sfGFP-sens* transgenes were created by combinatorial deletion of the two identified binding sites in the 607 nt *sens* 3 'UTR as had been described previously (Cassidy et al., 2013), so as to generate the *sfGFP-sens-m1*, *sfGFP-sens-m2,* and *sfGFP-sens-m1m2* mutant transgenes. All *sfGFP-sens* P[acman] constructs were integrated at the PBacy+-attP-3BVK00037 (22A3) landing site by phiC31 recombination (Venken et al., 2006). Transgenic alleles rescue the $sens^{E1}$ and $sens^{E2}$ mutations (Cassidy et al., 2013; Venken et al., 2006). All experimental animals had two copies of a *sfGFP-sens* transgene in a $sens^{E1}/sens^{E2}$ background.. Thus, the only Sens protein expressed from these animals came from the transgenes.

Fluorescence microscopy and quantification

All fluorescence microscopy experiments used female animals. Animals were staged based on morphology. The larval-pupal transition stage is one marked by the animals appearing as white prepupae. This stage lasts for only 45-60 minutes. The late larval stage is one marked by the animals as large wandering larvae with clear guts. This stage lasts for about 1-2 hours. Wing discs from staged animals were dissected out in ice-cold Phosphate Buffered Saline (PBS). Discs were fixed in

4% (w/v) paraformaldehyde in PBS for 20 minutes at 25°C, and washed with PBS containing 0.3% Tween-20. Then they were stained with 0.5 µg/ml 4′,6-diamidino-2-phenylindole (DAPI, Thermo Scientific), and mounted in Vectashield (Vector Labs). Discs were mounted apical-side up, and imaged with identical settings using a Leica TCS SP5 confocal microscope. Images were acquired at 100x magnification, at 2048 x 2048 resolution, with a 75 nm x-y pixel size, and 0.42 µm z separation. Scans were collected bidirectionally at 400 MHz, and 6x line averaged. Wing discs of different genotypes were mounted on the same microscope slide, and imaged in the same session, for consistency in data quality. Image segmentation, quantification, and conversion to absolute numbers of Sens molecules was carried out using a custom computational pipeline as described (Giri et al., 2020). On average, 1,000 ± 200 Sens-positive cells were quantified from each imaged wing disc, and a total of 6 to 12 discs were imaged for each condition.

Immunohistochemistry

Discs were dissected, and fixed as above, before incubating with the primary antibodies of interest. Tissues were washed thrice for 5-10 minutes each, and incubated with the appropriate fluorescent secondary antibodies (diluted 1:250) for 1 hour. They were then stained with DAPI, washed in PBS-Tween, and mounted for imaging. Guinea pig anti-Sens antibody (gift from H. Bellen) was used at 1:1000 dilution. Mouse monoclonal anti-Wg 4D4 was obtained from the Developmental Studies Hybridoma Bank (DSHB) and used at a 1:25 dilution.

Cell distance estimation

Cell distances from the wing pouch dorsoventral midline were estimated by approximating a curved line representing the midline for each disc, and subsequently calculating the shortest straight-line distance between this approximated margin and the cell centroid as obtained from the automated image-quantification pipeline.

Temperature perturbation

Animals were grown in either 18˚C or 29˚C incubators until the desired stage of development was reached, at which point the wing discs were rapidly dissected, fixed and processed as described above.

Mixture model analysis and probability density functions

Probability density functions were calculated using a kernel density estimation. The appropriate value for the bandwidth parameter was estimated using either Scott's rule or Silverman's rule. Both estimators were independently used and both gave highly similar results (Fig. S3). For mixture model analysis, the R package mixtools and Python package sklearn were used. Single-cell Sens distributions in individual discs were assumed to be composed of *k* Guassian sub-distributions. The best-fit value of *k* was determined by testing mixture models with different values of *k* and comparing the change in relative information score. Both the Akaike Information Criterion (AIC) and Bayesian Information Criterion (BIC) were evaluated since the AIC score is known to be biased towards over-parameterization. The least parametrized model that yielded sufficiently low AIC and BIC scores across several discs from both larval and larval to pupal transition stages was determined empirically to be 4. Using parameter $k = 4$, the mean, standard deviation and proportion were determined for each sub-population within a population of Sens-positive cells obtained from each individual wing pouch. The values of mean, standard deviation, and proportion were averaged from six to twelve wing pouches per treatment (Table 1). We observed that each subpopulation mean was separated from the adjacent subpopulation's mean by a value greater than the sum of their standard deviations (Table 1). Moreover, each sub-population's coefficient of variation was fairly similar to the other sub-populations', regardless of sample or stage (Table 1). The number of cells in each state was calculated by assuming that each cell appears in approximately 4 out of 5 optical slices imaged per pouch, and multiplying the total number of Sens-positive cells in the pouch by the proportion value of each state for that pouch.

Mathematical model for patterning

The mathematical model for self-organization of *Drosophila* proneural tissue and fate selection is as described by Corson et. al. (2017) as

$$\tau\, du/dt = f(u-s) - u + \eta(t)$$

Here u describes the state of each cell and can range from 0 (low u or Epidermal-fate) to 1 (high u or SOP fate). We assume u represents the fractional concentration of fate determinant Sens molecules. Inhibitory signals received from neighbor cells are summed and represented as s and τ is the time-scale of cell dynamics. The functional form and parameter values describing the function $f(u-s)$ which integrates the activating and inhibiting signals, were kept identical to Corson et al (2017). The model was simplified to a 1-dimensional row of 20 cells with periodic boundary conditions, and 100 simulations were run in parallel for each condition. The Brownian noise term which relates to $\eta(t)$ was set at 1% relative to u (process noise = 0.01) for the simulation results presented in Figure 2. This term describes the level of stochasticity in the dynamics of cell state u encoded in the model. A total of 250 time-steps were simulated in order to ensure convergence, however cell-state resolution was generally observed within 25-50 time steps, therefore Figure 2 shows the time-evolving distribution at every third time-step in the series from steps 1-30. Code and all parameter values for explicitly generating the simulations and figure plots is provided in supplementary materials.

Acknowledgements

Fly stocks from Hugo Bellen, Fen Biao Gao, and the Bloomington Drosophila Stock Center are gratefully appreciated. Antibodies were gifts from Hugo Bellen and purchases from the Developmental Studies Hybridoma Bank. We thank Jessica Hornick and the Biological Imaging Facility for help with imaging. Financial support was provided from the Northwestern Data Science Initiative (R.G.), Robert

H. Lurie Comprehensive Cancer Center (R.G.), NIH (R35GM118144, R.W.C.), NSF (1764421, R.W.C.), and the Simons Foundation (597491, R.W.C.).

Author Contributions

The experimental work was conceived by R.G. and R.W.C.. Experimental work was performed by R.G. and S.B., under the supervision of R.W.C. Mathematical modeling was performed by R.G. All data and model analysis were performed by R.G. under the supervision of R.W.C. The manuscript was written by R.G. and R.W.C.

Competing Interests

The authors declare no competing financial interests.

Table 1. State values from mixture modeling individual wing pouches from n > 6 wing pouches per stage. Note the difference in means between adjacent states is greater than the sum of their standard deviations, suggesting the states are well separated in the models.

Stage	State	Proportion	Mean Sens protein number	Standard deviation of Sens protein number	Coefficient of Variation (Mean / Standard Deviation)
Larval	1	0.22	56.42	9.93	0.18
	2	0.22	114.94	37.09	0.32
	3	0.34	336.57	135.39	0.40
	4	0.22	799.35	283.19	0.35
Larval-Pupal Transition	1	0.19	115.40	31.85	0.28
	2	0.37	315.05	124.74	0.40
	3	0.39	875.18	346.47	0.40
	4	0.05	2262.81	818.87	0.36

References

Acar, M., Jafar-Nejad, H., Giagtzoglou, N., Yallampalli, S., David, G., He, Y., Delidakis, C., and Bellen, H.J. (2006). Senseless physically interacts with proneural proteins and functions as a transcriptional co-activator. Development *133*, 1979-1989.

Alexandre, C., Baena-Lopez, A., and Vincent, J.P. (2014). Patterning and growth control by membrane-tethered Wingless. Nature *505*, 180-185.

Antolovic, V., Lenn, T., Miermont, A., and Chubb, J.R. (2019). Transition state dynamics during a stochastic fate choice. Development *146*.

Bakker, R., Mani, M., and Carthew, R.W. (2020). The Wg and Dpp morphogens regulate gene expression by modulating the frequency of transcriptional bursts. Elife *9:e56076*.

Carthew, R.W., and Sontheimer, E.J. (2009). Origins and mechanisms of miRNAs and siRNAs. Cell *136*, 642-655.

Cassidy, J.J., Jha, A.R., Posadas, D.M., Giri, R., Venken, K.J.T., Ji, J., Jiang, H., Bellen, H.J., White, K.P., and Carthew, R.W. (2013). miR-9a minimizes the phenotypic impact of genomic diversity by buffering a transcription factor. Cell *155*, 1556-1567.

Chang, H.H., Hemberg, M., Barahona, M., Ingber, D.E., and Huang, S. (2008). Transcriptome-wide noise controls lineage choice in mammalian progenitor cells. Nature *453*, 544-547.

Claeskens, G., and Hjort, N.L. (2008). Model Selection and Model Averaging (Cambridge, UK: Cambridge University Press).

Corson, F., Couturier, L., Rouault, H., Mazouni, K., and Schweisguth, F. (2017). Self-organized Notch dynamics generate stereotyped sensory organ patterns in *Drosophila*. Science *356*.

Corson, F., and Siggia, E.D. (2012). Geometry, epistasis, and developmental patterning. Proc Natl Acad Sci U S A *109*, 5568-5575.

Eivers, E., Fuentealba, L.C., Sander, V., Clemens, J.C., Hartnett, L., and De Robertis, E.M. (2009). Mad is required for Wingless signaling in wing development and segment patterning in *Drosophila*. PLoS One *4*, e6543.

Freedman, S.L., Xu, B., Goyald, G., and Mani, M. (2021). Revealing cell-fate bifurcations from transcriptomic trajectories of hematopoiesis. bioRxiv doi.org/10.1101/2021.05.03.442465.

Frick, C.L., Yarka, C., Nunns, H., and Goentoro, L. (2017). Sensing relative signal in the Tgf-beta/Smad pathway. Proc Natl Acad Sci U S A *114*, E2975-E2982.

Garcia-Bellido, A., and de Celis, J.F. (2009). The complex tale of the *achaete-scute* complex: a paradigmatic case in the analysis of gene organization and function during development. Genetics *182*, 631-639.

Giri, R., Papadopoulos, D.K., Posadas, D.M., Potluri, H.K., Tomancak, P., Mani, M., and Carthew, R.W. (2020). Ordered patterning of the sensory system is susceptible to stochastic features of gene expression. Elife *9:e53638*.

Goentoro, L., and Kirschner, M.W. (2009). Evidence that fold-change, and not absolute level, of beta-catenin dictates Wnt signaling. Mol Cell *36*, 872-884.

Handke, B., Szabad, J., Lidsky, P.V., Hafen, E., and Lehner, C.F. (2014). Towards long term cultivation of *Drosophila* wing imaginal discs in vitro. PLoS One *9*, e107333.

Hinz, U., Giebel, B., and Campos-Ortega, J.A. (1994). The basic-helix-loop-helix domain of *Drosophila* Lethal of Scute protein is sufficient for proneural function and activates neurogenic genes. Cell *76*, 77-87.

Huang, S., Eichler, G., Bar-Yam, Y., and Ingber, D.E. (2005). Cell fates as high-dimensional attractor states of a complex gene regulatory network. Phys Rev Lett *94*, 128701.

Imayoshi, I., Isomura, A., Harima, Y., Kawaguchi, K., Kori, H., Miyachi, H., Fujiwara, T., Ishidate, F., and Kageyama, R. (2013). Oscillatory control of factors determining multipotency and fate in mouse neural progenitors. Science *342*, 1203-1208.

Jafar-Nejad, H., Acar, M., Nolo, R., Lacin, H., Pan, H., Parkhurst, S.M., and Bellen, H.J. (2003). Senseless acts as a binary switch during sensory organ precursor selection. Genes Dev *17*, 2966-2978.

Jafar-Nejad, H., Tien, A.C., Acar, M., and Bellen, H.J. (2006). Senseless and Daughterless confer neuronal identity to epithelial cells in the *Drosophila* wing margin. Development *133*, 1683-1692.

Kelso, J.A. (2012). Multistability and metastability: understanding dynamic coordination in the brain. Philos Trans R Soc Lond B Biol Sci *367*, 906-918.

Klein, A.M., Mazutis, L., Akartuna, I., Tallapragada, N., Veres, A., Li, V., Peshkin, L., Weitz, D.A., and Kirschner, M.W. (2015). Droplet barcoding for single-cell transcriptomics applied to embryonic stem cells. Cell *161*, 1187-1201.

Kooh, P.J., Fehon, R.G., and Muskavitch, M.A. (1993). Implications of dynamic patterns of Delta and Notch expression for cellular interactions during *Drosophila* development. Development *117*, 493-507.

Lee, R.E., Walker, S.R., Savery, K., Frank, D.A., and Gaudet, S. (2014). Fold change of nuclear NF-kappaB determines TNF-induced transcription in single cells. Mol Cell *53*, 867-879.

Levine, J.H., Lin, Y., and Elowitz, M.B. (2013). Functional roles of pulsing in genetic circuits. Science *342*, 1193-1200.

Li, Y., Wang, F., Lee, J.A., and Gao, F.B. (2006). MicroRNA-9a ensures the precise specification of sensory organ precursors in *Drosophila*. Genes Dev *20*, 2793-2805.

Marco, E., Karp, R.L., Guo, G., Robson, P., Hart, A.H., Trippa, L., and Yuan, G.C. (2014). Bifurcation analysis of single-cell gene expression data reveals epigenetic landscape. Proc Natl Acad Sci U S A *111*, E5643-5650.

Nolo, R., Abbott, L.A., and Bellen, H.J. (2000). Senseless, a Zn finger transcription factor, is necessary and sufficient for sensory organ development in *Drosophila*. Cell *102*, 349-362.

Nolo, R., Abbott, L.A., and Bellen, H.J. (2001). *Drosophila Lyra* mutations are gain-of-function mutations of *senseless*. Genetics *157*, 307-315.

Olsson, A., Venkatasubramanian, M., Chaudhri, V.K., Aronow, B.J., Salomonis, N., Singh, H., and Grimes, H.L. (2016). Single-cell analysis of mixed-lineage states leading to a binary cell fate choice. Nature *537*, 698-702.

Rand, D.A., Raju, A., Saez, M., Corson, F., and Siggia, E.D. (2021). Geometry of gene regulatory dynamics. Proc Natl Acad Sci U S A *118,* e2109729118.

Thomas, P., Popovic, N., and Grima, R. (2014). Phenotypic switching in gene regulatory networks. Proc Natl Acad Sci U S A *111*, 6994-6999.

Venken, K.J., He, Y., Hoskins, R.A., and Bellen, H.J. (2006). P[acman]: a BAC transgenic platform for targeted insertion of large DNA fragments in *D. melanogaster*. Science *314*, 1747-1751.

Waddington, C.H. (1957). The Strategy of the Genes (George Allen and Unwin Ltd.).

Zartman, J., Restrepo, S., and Basler, K. (2013). A high-throughput template for optimizing *Drosophila* organ culture with response-surface methods. Development *140*, 667-674.

Zecca, M., Basler, K., and Struhl, G. (1996). Direct and long-range action of a wingless morphogen gradient. Cell *87*, 833-844.

Figure Legends

Figure 1. Sensory organ fate selection at the developing *Drosophila* wing margin. (A) An adult wing with the anterior margin on top. Inset shows a magnified view of the margin with slender chemosensory bristles marked. Stout mechanosensory bristles occupy the extreme margin edge. (B) Schematic of the wing imaginal disc as it grows during larval stages until pupation. Embedded in the disc is the wing pouch as indicated. A, anterior; P, posterior; D, dorsal; V, ventral. (C) Schematic of Sens expression in the wing pouch at the larval-pupal transition stage. (D) Sens protein fluorescence in a wing pouch. Note the periodic bright spots of fluorescence denoting SOPs. (E,F) In the late larval stage, two stripes of Sens protein (white in E and purple in F) are induced by Wg protein (green in F). Panel E is a lower magnification view of the pouch. (G,H) In the larval-pupal transition stage, the two

stripes of Sens protein (white in G and purple in H) evolve to have within them two periodic rows of SOPs. Panel G is a lower magnification view of the pouch.

Figure S1. Sens expression dynamics. (A) Steps in the process of resolving cell fate decisions with Sens. (B) Schematic of the gene regulatory network that operates in proneural cells at the anterior wing margin. (C) Cells undergoing the sensory versus epidermal fate decision are thought to exhibit bistability. An intermediate level of Sens expression is an unstable cell state can resolve into one of two stable states: a high Sens expressing SOP state, or a low Sens expressing epidermal state.

Figure 2. A mathematical model for Sens pattern formation. (A) Each cell in the 1D cell array reaches an unstable steady state of intermediate value for u. Cells then bifurcate to zero or maximal values of u, corresponding to stable steady states. (B) Single-cell traces for u as simulations evolve over time. A total of 20 simulated cells are shown comprising a single simulation run. (C) A representative 1D array of 20 cells shown as they vary in u over simulation time. Note the "errors" in periodic patterning between cells 6-7 and 10-11. Such patterning errors are generated due to the noise term present in the model. The noise parameter was set to 1% relative to u. A lower noise parameter value results in fewer "errors". (D) The distribution of the cell state variable u in model simulations over time. A total of 100 simulations with 20 cells each (total 2,000 cells) were run with identical parameters. At discrete time steps, simulations were tallied for their values of u. The arrow marks the time at which the unstable steady state begins to bifurcate. In the model, Sens protein level is synonymous with the cell state variable u.

Figure S2. The structure of the sfGFP-sens transgene. Note that is is composed of 19.2 kb of genomic DNA, of which only a small portion encodes the *sens* transcription unit. However, the genomic fragment appears to contain all of the *cis*-regulatory DNA needed for faithful *sens* expression and function.

Figure 3. Sens-positive proneural cells display four-state multimodality. (A,B) A histogram of sfGFP-Sens protein number per cell for 5,000 randomly sampled cells is shown in each panel. Cells were sampled at the late larval stage (A) or the larval-pupal transition stage (B). (C) Sens expression profiles (density plots) derived from three representative wing pouches collected at the larval stage. (D) AIC and BIC scores were independently derived for Gaussian mixture models of the Sens data from an individual wing pouch. The AIC and BIC assess the relative quality of statistical models built with different values of the parameter *k*, which defines the number of states within a parent distribution. Models with a *k* value that generates the lowest AIC and BIC scores are deemed to be best-fit, in that they are best at describing the data without overfitting by having higher values of *k*. (E) Mean Sens protein number for cells in the four states. Each dot represents an estimate derived from one wing pouch sample. Wing pouches are from the larval (blue) and larval-pupal (red) stages of development. Mean and standard deviations for the pouch replicates are shown with boxplots. The difference in Sens number between larval and larval-pupal stages for each state were all statistically significant ($p < 0.02$, Wilcoxon test). (F) Estimated number of cells within each state for the four states. Each dot represents an estimate derived from one wing pouch sample. Wing pouches are from the larval (blue) and larval-pupal (red) stages of development. Mean and standard deviations for the pouch replicates are shown with boxplots. The difference in cell number between larval and larval-pupal stages for state 1 was not significant ($p = 0.081$) but for states 2,3, and 4, were all statistically significant ($p < 0.005$, Wilcoxon test).

Figure S3. Kernel density estimations of three populations of Sens-positive cells. From left to right, each chart displays a population of Sens-positive cells from an individual wing pouch. To show that the probability density distribution qualitatively appears multimodal regardless of bandwidth parameter selection, the parameter was chosen either using Scott's (top) or Silverman's (bottom) rule.

Figure S4. AIC and BIC scores for Gaussian mixture models with different numbers of states in the model. Sens data from individual wing pouches were independently assessed using the AIC and BIC scores. These tested the relative quality of statistical models built with different values of the parameter *k*, which defines the number of states within a parent distribution. Models with a *k* value that generates the lowest AIC and BIC score are deemed to be best-fit, in that they are best at describing the data without overfitting by having higher values of *k*. Shown in each panel are scores for individual wing pouch samples used in experiments described in Figure 3.

Figure 4. Cells in Sens expression states are patterned within each proneural stripe. (A) Sens expression level is weakly correlated with distance from the dorsoventral midline. Single cells from three representative wing pouches at the larval stage (top) and larval-pupal transition stage (bottom) are plotted for their distance to the midline on the x-axis and Sens protein number on the y-axis. (B,C) Single cells were classified into one of the states according to their Sens protein number relative to the mean Sens number in states. Cells are color coded according to state classification as shown, and plotted as a function of their distance to the midline on the x-axis and Sens protein number on the y-axis. Shown are cells analyzed from one wing pouch taken at the larval stage (B) or larval-pupal transition stage (C). (D) Half-violin plots of cells' distance to the dorsoventral midline according to their state classification. Cells from larval stage and larval-pupal transition stage are plotted together according to their state classification.

Figure S5. Estimation of the shortest distance from a cell to the dorsoventral midline. (A) A fluorescence image slice of a wing pouch expressing sfGFP-Sens is shown. To calculate cell distance from the midline, pixel coordinates making up the dorsoventral midline were estimated manually and delineated in white. (B) Cell-centroids of each segmented cell were mapped. Dorsal compartment cells are marked in gray, ventral in black for reference. Cell distance from the midline was calculated

as the shortest Euclidean distance from the cell centroid to the estimated midline and converted to micrometers based on the imaging scale factor.

Figure S6. Mutation of miR-9a binding sites in *sens* increases Sens protein output. (A) Sens expression patterns for different miR-9a binding-site mutant *sens* alleles. Fluorescence from sfGFP-Sens in larval-pupal wing pouches is shown. Sens expression was assayed for different combinations of miR-9a binding-site mutations in the *sens* 3'UTR in an endogenous *sens* null background. All four alleles rescue *sens* expression. Wild-type like transgene *sfGFP-sens* had both miR-9a sites intact, site 1 and site 2 were deleted in *sfGFP-sens-m1* and *sfGFP-sens-m2* alleles respectively. Both sites were deleted in allele *sfGFP-sens-m1m2*. (B,C) Cumulative density plots show the distributions of Sens protein number for cells expressing various *sens* alleles. Linear scale for Sens number is on the left, log scale is on the right. (B) Single-site mutants *sens-m1* and *sens-m2* are compared to wild-type *sens*. (C) Sens protein output increases when both miR-9a binding sites are deleted in *sens-m1m2*, relative to wild-type *sens*. (D) Sens protein output from the wild-type *sens* andmutant *sens-m1m2* alleles was measured in the presence (left) or absence (right) of the endogenous *mir-9a* gene. The cumulative density plot shows the difference in protein output between wild-type and mutant transgenes. When *mir-9a* is present, wild-type Sens expression is lower compared to the *m1m2* mutant. However, this difference is greatly diminished when endogenous miR-9a is not present.

Figure 5. Perturbation of Sens number per cell has little effect on cell-state properties. (A) Histograms of sfGFP-Sens protein number in 5,000 randomly sampled cells are shown. Dotted lines represent the median numbers for the populations. Cells were collected from larval-pupal cells expressing wild-type *sens* (top) or the miR-9a binding-site mutant allele *sens-m1m2* (bottom). (B) Sens protein number for cells in the four states. Each dot represents a mean estimate of protein number derived from one larval-pupal stage wing pouch. Wing pouches are from wildtype *sens* (blue) and *sens-m1m2* (red) alleles. Mean and standard deviations for the pouch replicates are shown with boxplots.

The differences in Sens number between *sens* and *sens-m1m2* for states 1 and 2 were not significant ($p > 0.10$, Wilcoxon test) but for states 3 and 4 they were significant ($p < 0.003$, Wilcoxon test). (C,D) Estimated number of cells within each state for the four states. Each dot represents an estimate derived from one wing pouch. Wing pouches are from wildtype *sens* (blue) and *sens-m1m2* (red) alleles. Mean and standard deviations for the pouch replicates are shown with boxplots. Cells were sampled at the larval (C) and larval-pupal transition (D) stages. The differences in cell number between *sens* and *sens-m1m2* for each state in (C) were not significant ($p > 0.09$, Wilcoxon test). The differences in cell number between *sens* and *sens-m1m2* for states 1, 3, and 4 in (D) were not significant ($p > 0.07$, Wilcoxon test) but for state 2 it was significant ($p = 0.02$, Wilcoxon test). (E) Histograms of sfGFP-Sens protein number in 5,000 randomly sampled cells are shown. Dotted lines represent the median numbers for the populations. Cells were collected from larval-pupal cells grown at 18°C (top) or 29°C (bottom). (F) Sens protein number for cells in the four states. Each dot represents a mean estimate of protein number derived from one larval-pupal stage wing pouch. Wing pouches are from animals grown at 18°C (blue) and 29°C (red). Mean and standard deviations for the pouch replicates are shown with boxplots. The differences in Sens number between 18°C and 29°C for each state were all significant ($p < 0.0025$, Wilcoxon test). (G) Estimated number of cells within each state for the four states. Each dot represents an estimate derived from one larval-pupal stage wing pouch. Wing pouches are from animals grown at 18°C (blue) and 29°C (red). Mean and standard deviations for the pouch replicates are shown with boxplots. The differences in cell number between 18°C and 29°C for states 1, 3, and 4 were not significant ($p > 0.30$, Wilcoxon test) but for state 2 it was significant ($p = 0.04$, Wilcoxon test).

Figure S7. Combined change in miR-9a regulation and growth temperature have little effect on cell-state properties. (A) Representative larval-pupal wing pouch images showing sfGFP-Sens expression from animals raised at either 18°C or 29°C. (B) Sens protein number for cells in the four states. Each dot represents a mean estimate of protein number derived from one larval-pupal stage wing pouch. Wing pouches are from wildtype *sens* animals grown at 18°C (blue) or *sens-m1m2* mutant

animals grown at 29°C (red). Mean and standard deviations for the pouch replicates are shown with boxplots. The differences in Sens number between *sens* at 18°C and *sens-m1m2* at 29°C for each state were all significant ($p < 0.001$, Wilcoxon test). (C) Estimated number of cells within each state for the four states. Each dot represents an estimate derived from one larval-pupal stage wing pouch. Wing pouches are from wildtype *sens* animals grown at 18°C (blue) or *sens-m1m2* mutant animals grown at 29°C (red). Mean and standard deviations for the pouch replicates are shown with boxplots. The differences in cell number between *sens* at 18°C and *sens-m1m2* at 29°C for each state were not significant ($p > 0.15$, Wilcoxon test).

Figure 6. Relative ratios of Sens number and state models. (A) Ratio of the mean Sens number in cells that belong in adjacent states. Each dot corresponds to the ratio calculated specifically for a particular combination of experimental conditions, i.e. developmental stage, miR-9a regulation, growth temperature. All wing pouch replicates for each condition were averaged to derive these ratios. The mean and standard deviation of the ratios for each pair of neighboring states are shown. There are no statistically significant differences between the averaged ratios (shown are *p*-values from two-tailed t tests). However, the ratios observed in 29°C wing pouches are consistently higher than for the other conditions, as indicated. This difference is significant ($p = 0.0002$, two-tailed t test). (B,C) Two alternative models for how cells transition to and from metastable states. (B) Cells transition from a ground state to any one of four metastable states. They then either relax back to the ground state or transition to an SOP state with some likelihood, in this example with only state 4 being permissive for transition to the SOP state. Other scenarios are also possible. (C) Cells transition from a ground state to a particular metastable state, and following this, they transition to and from all of the other metastable states with some likelihood. In this example, only state 1 cells can relax back to the ground state and only state 4 cells can transition to an SOP state, but many other scenarios are equally plausible.

Figure 1

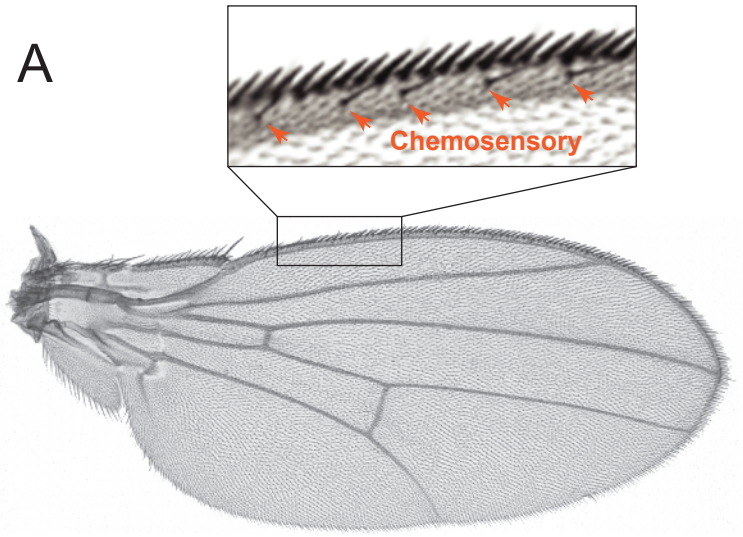

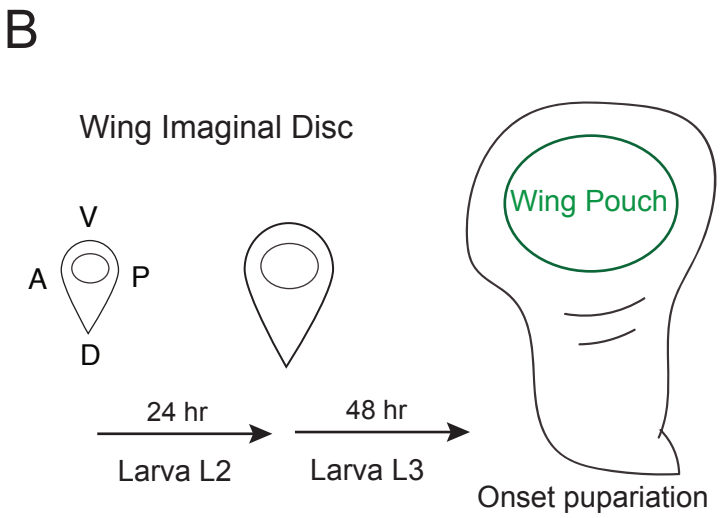

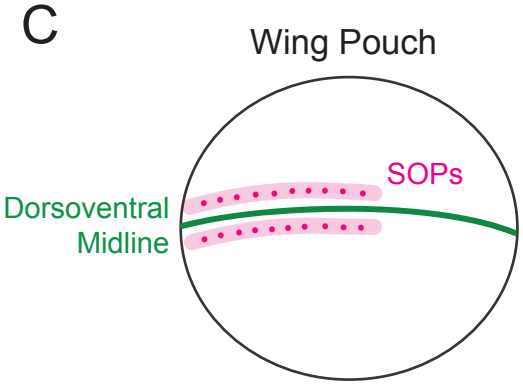

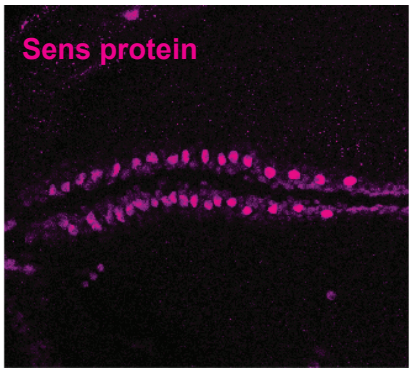

Late L3 Larval Stage

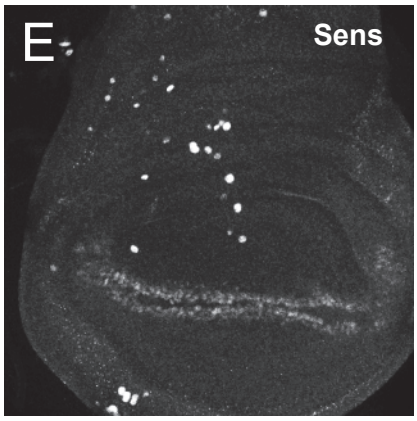

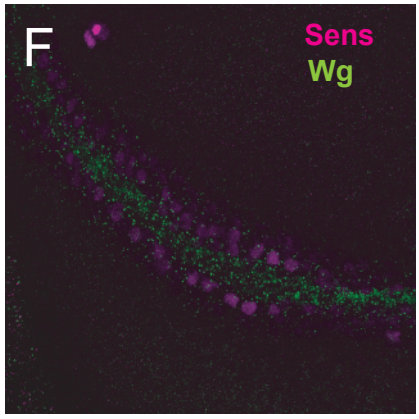

Larval-Pupal Transition Stage

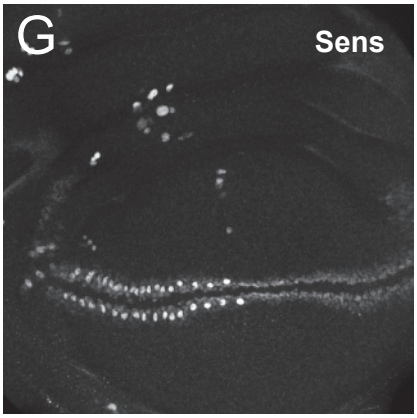

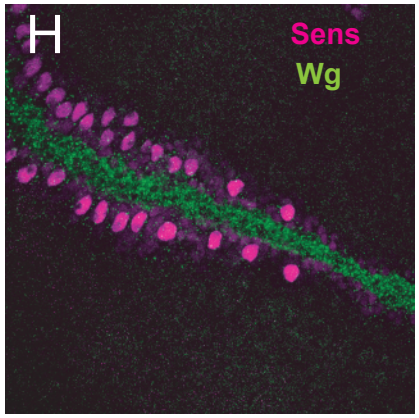

Figure S1

A

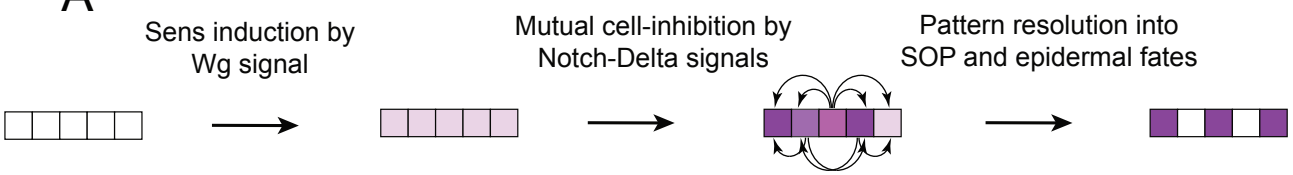

B

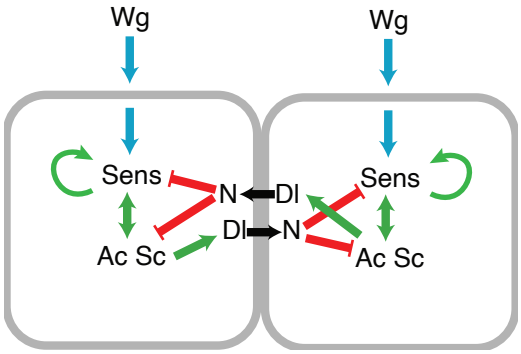

C

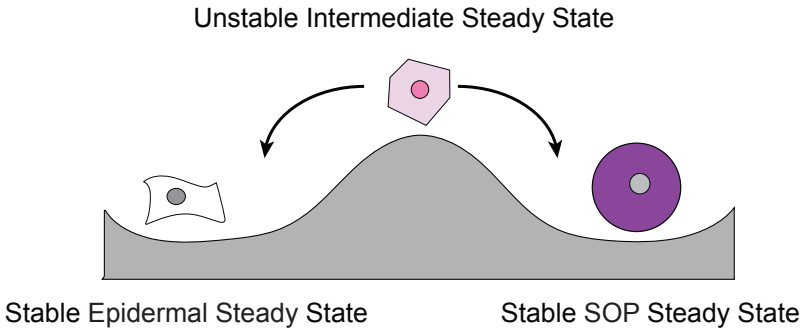

Figure 2

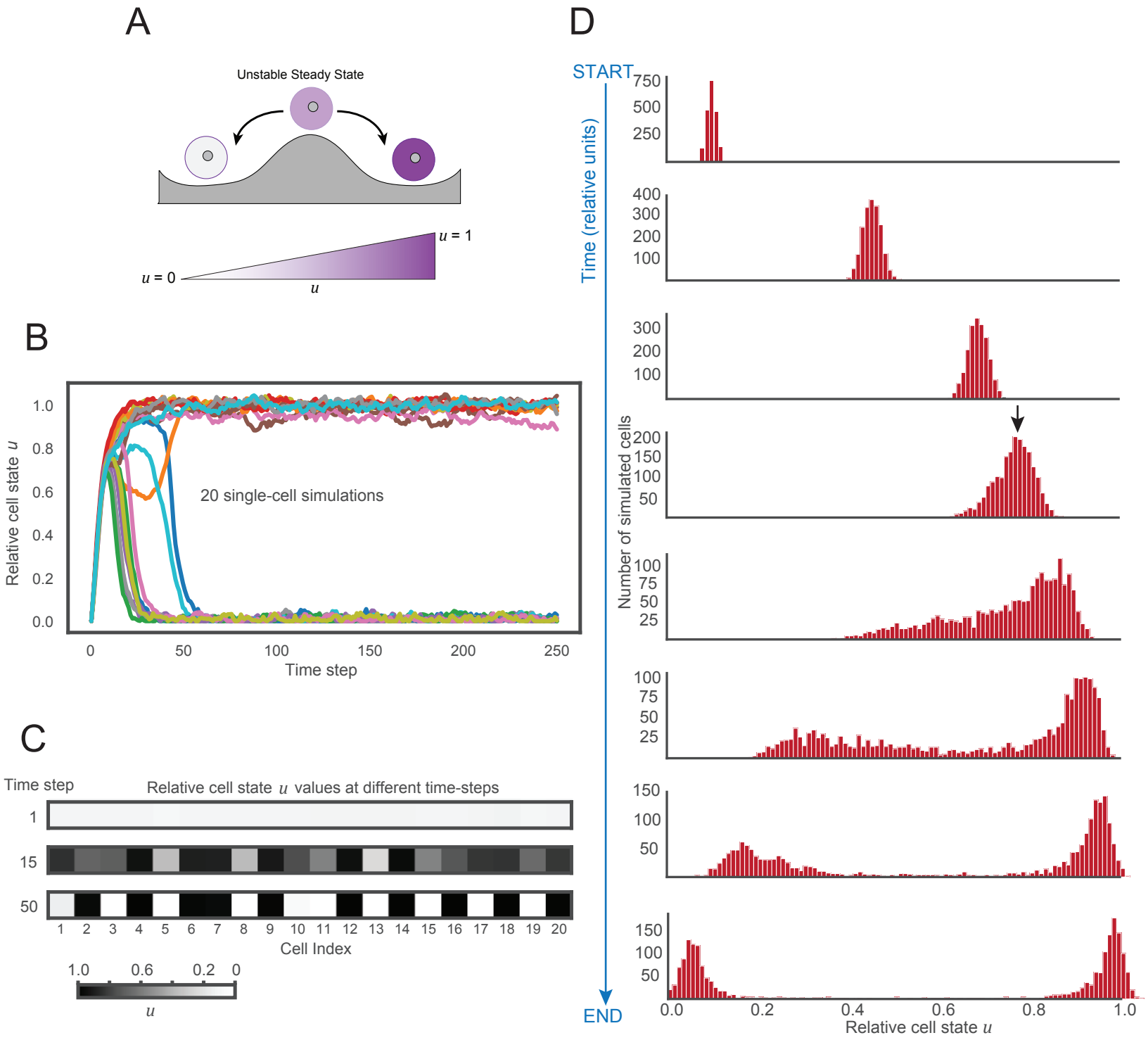
A
Unstable Steady State
u = 1
u = 0
u
B
Relative cell state u
1.0
0.8
0.6
0.4
0.2
0.0
20 single-cell simulations
0
50
100
150
200
250
Time step
C
Time step
Relative cell state u values at different time-steps
1
15
50
1 2 3 4 5 6 7 8 9 10 11 12 13 14 15 16 17 18 19 20
Cell Index
1.0 0.6 0.2 0
u
D
START
END
Time (relative units)
Number of simulated cells
750
500
250
400
300
200
100
300
200
100
200
150
100
50
100
75
50
25
100
75
50
25
150
100
50
150
100
50
0.0
0.2
0.4
0.6
0.8
1.0
Relative cell state u

Figure S2

Figure 3

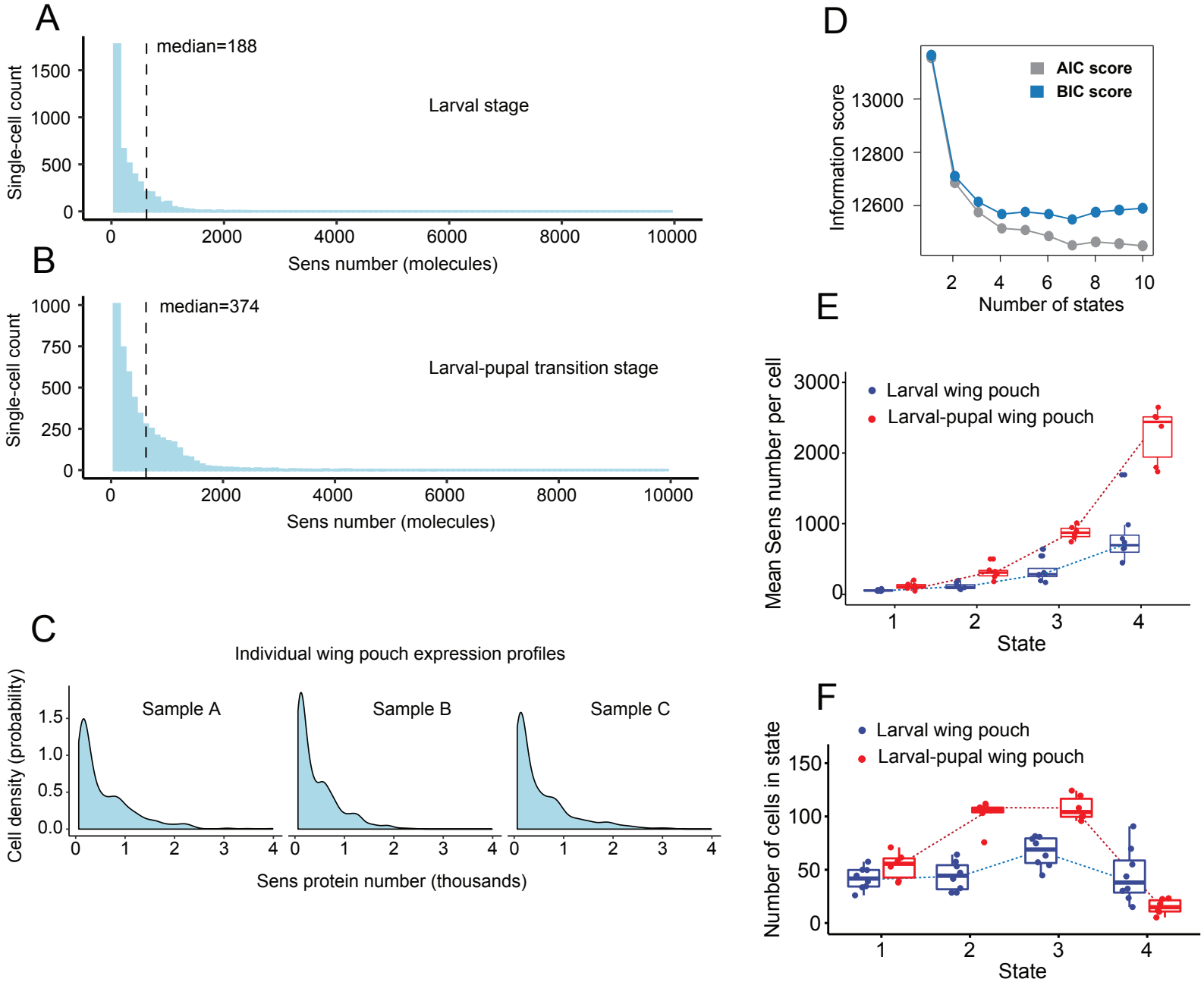
A
median=188
Larval stage
Single-cell count
1500
1000
500
0
0
2000
4000
6000
8000
10000
Sens number (molecules)
B
median=374
Larval-pupal transition stage
Single-cell count
1000
750
500
250
0
0
2000
4000
6000
8000
10000
Sens number (molecules)
C
Individual wing pouch expression profiles
Sample A
Sample B
Sample C
Cell density (probability)
1.5
1.0
0.5
0.0
0
1
2
3
4
Sens protein number (thousands)
D
AIC score
BIC score
Information score
13000
12800
12600
2
4
6
8
10
Number of states
E
Larval wing pouch
Larval-pupal wing pouch
Mean Sens number per cell
3000
2000
1000
0
1
2
3
4
State
F
Larval wing pouch
Larval-pupal wing pouch
Number of cells in state
150
100
50
0
1
2
3
4
State

Figure S3

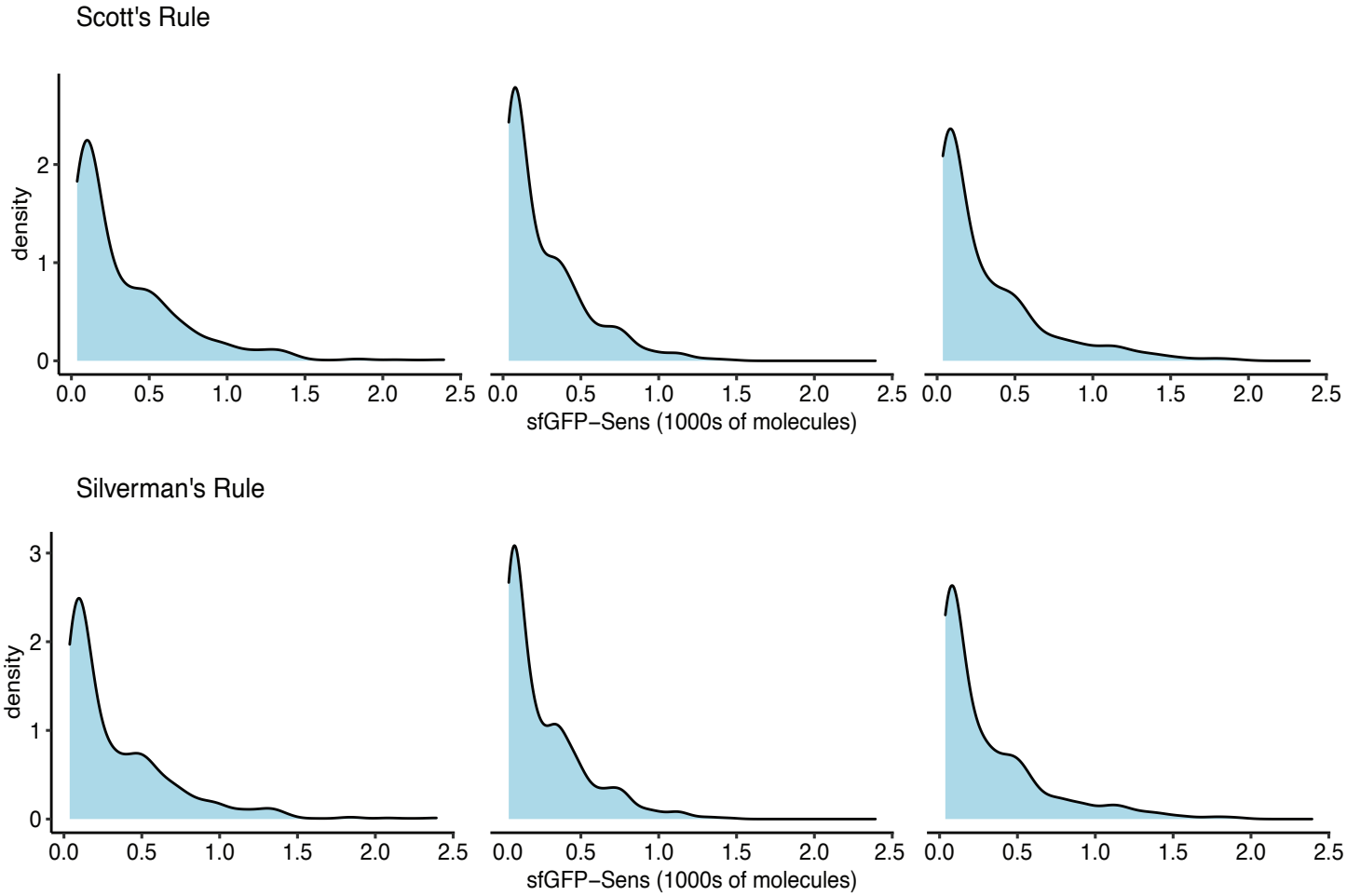
Scott's Rule
density
0
1
2
0.0
0.5
1.0
1.5
2.0
2.5
sfGFP−Sens (1000s of molecules)
Silverman's Rule
density
0
1
2
3
0.0
0.5
1.0
1.5
2.0
2.5
sfGFP−Sens (1000s of molecules)

Figure S4

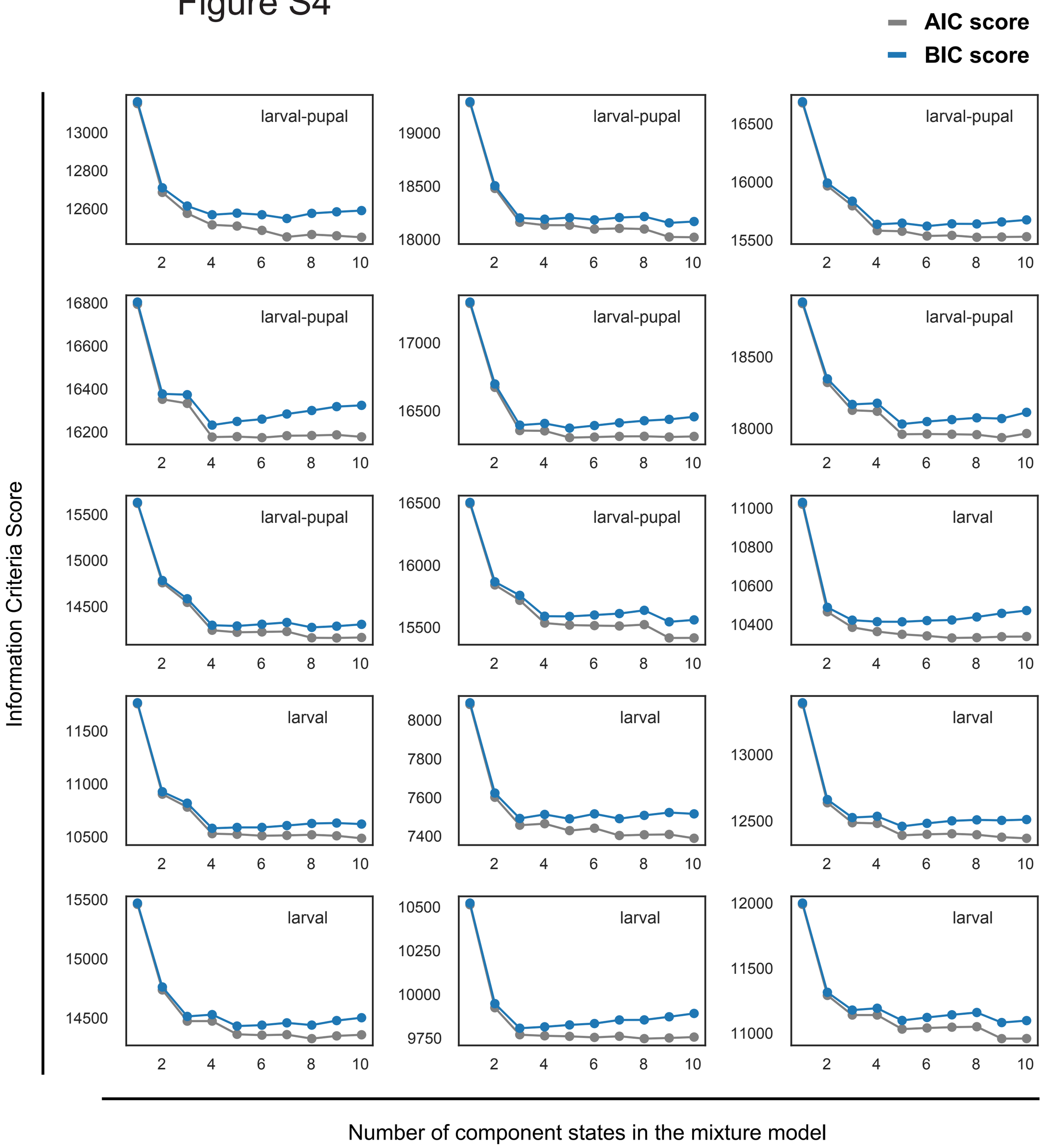
AIC score
BIC score
Information Criteria Score
Number of component states in the mixture model
larval-pupal
larval
13000
12800
12600
19000
18500
18000
16500
16000
15500
16800
16600
16400
16200
17000
16500
18500
18000
15500
15000
14500
16500
16000
15500
11000
10800
10600
10400
11500
11000
10500
8000
7800
7600
7400
13000
12500
15500
15000
14500
10500
10250
10000
9750
12000
11500
11000
2
4
6
8
10

Figure 4

A

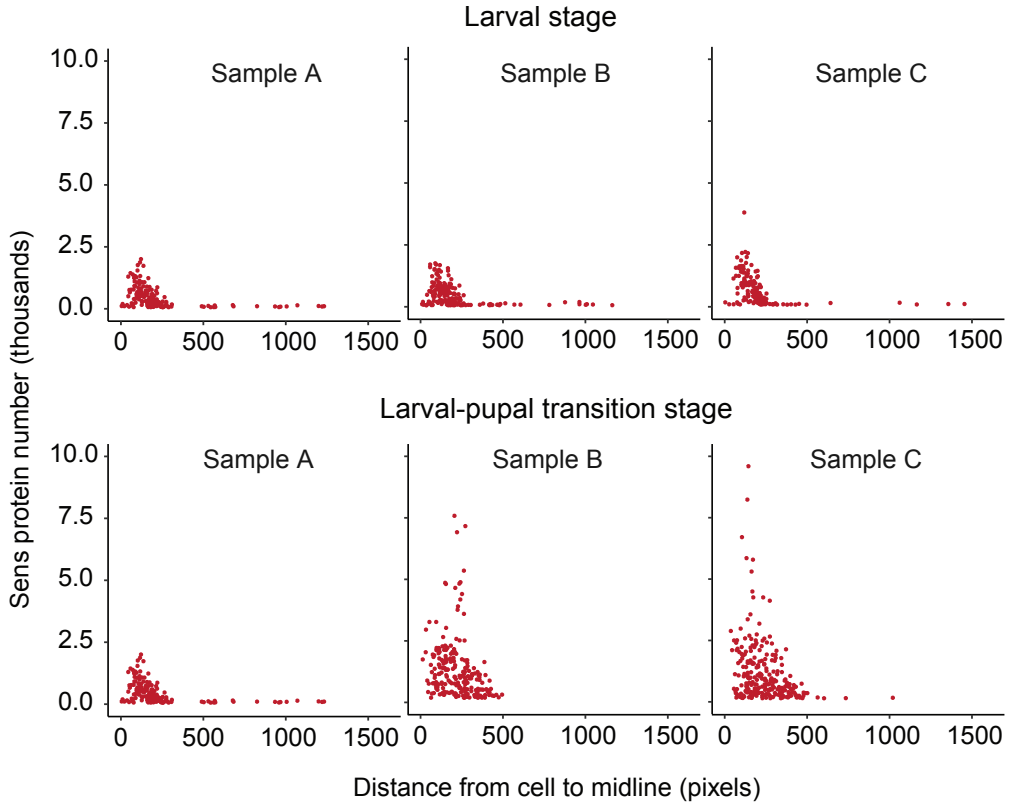

B

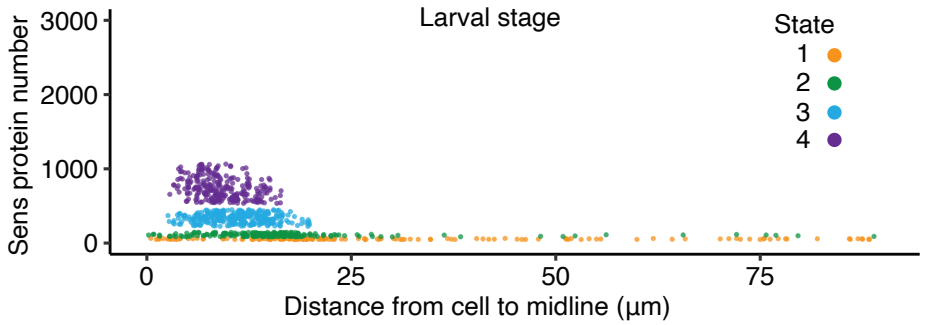

C

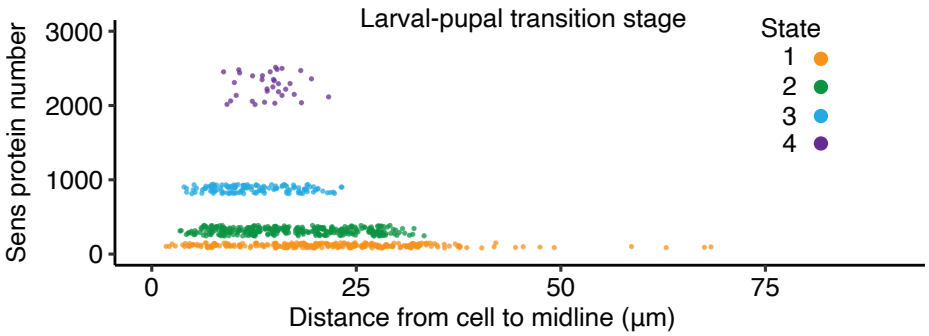

D

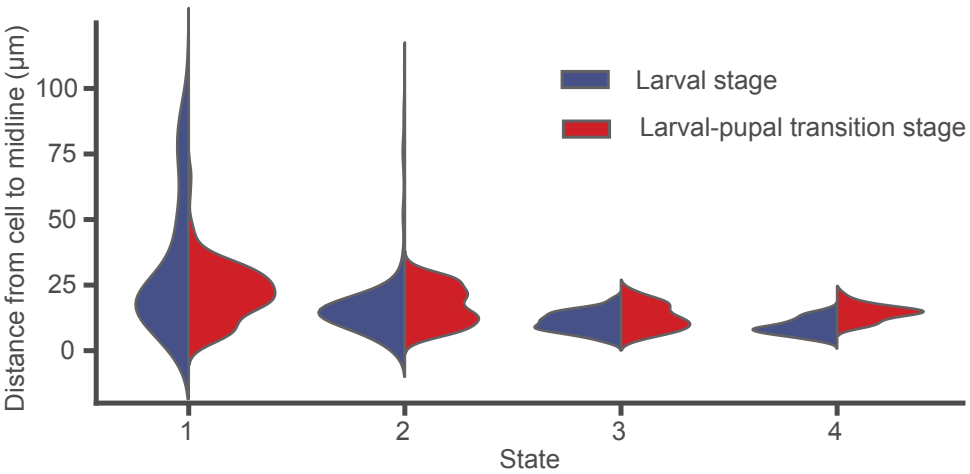

Figure S5

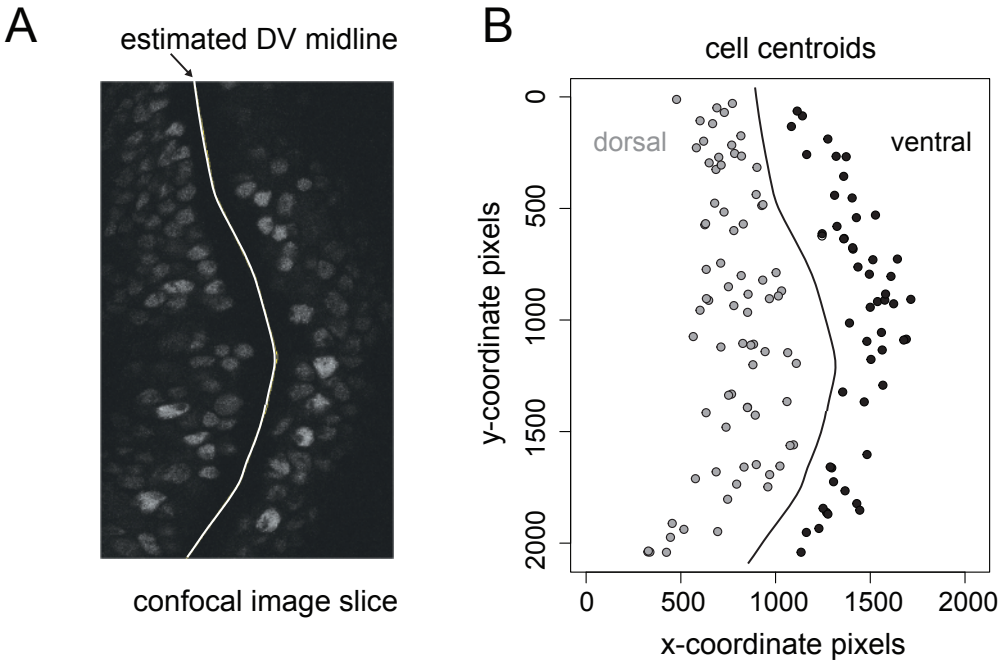
A
estimated DV midline
confocal image slice
B
cell centroids
dorsal
ventral
y-coordinate pixels
x-coordinate pixels
0
500
1000
1500
2000

A

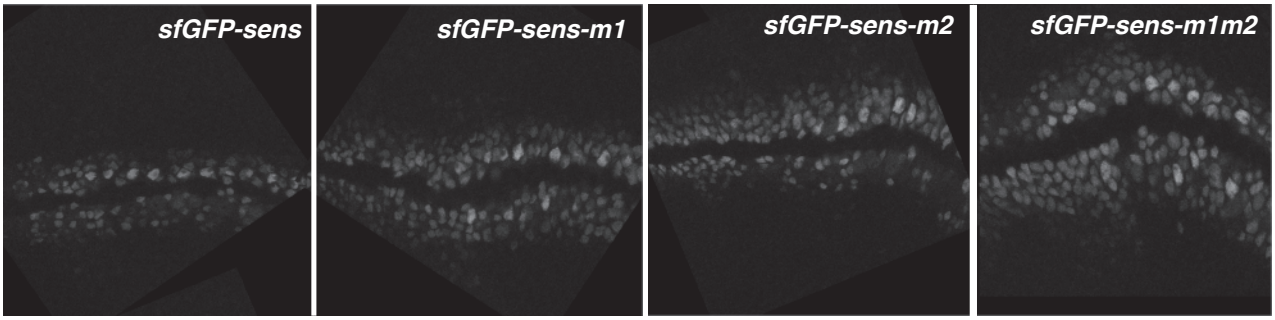

Figure S6

B

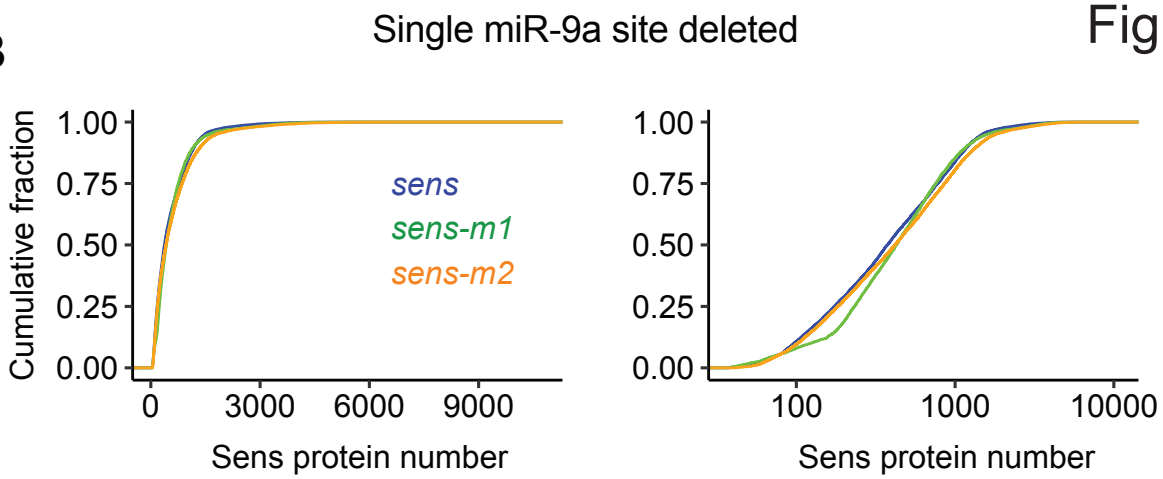

C

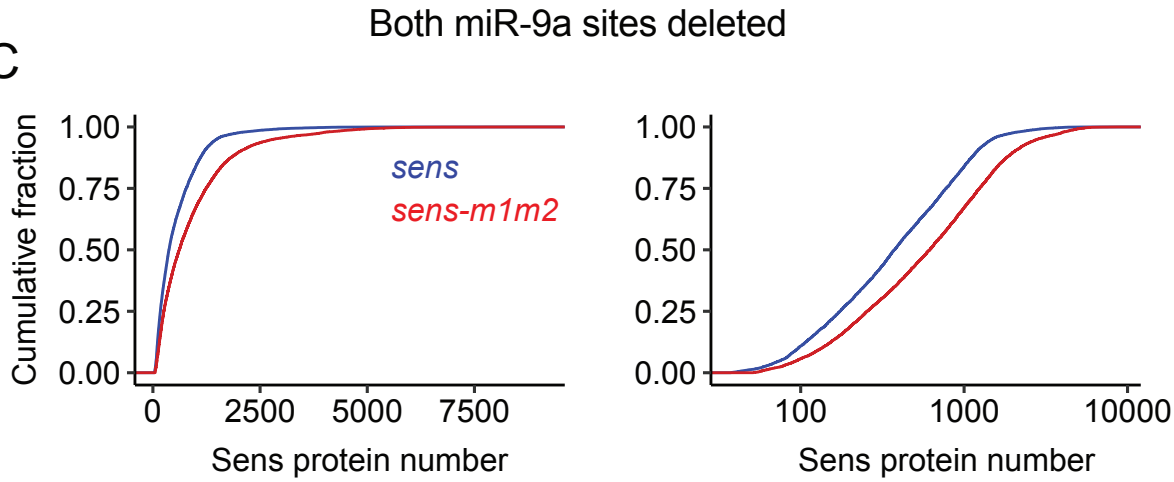

D

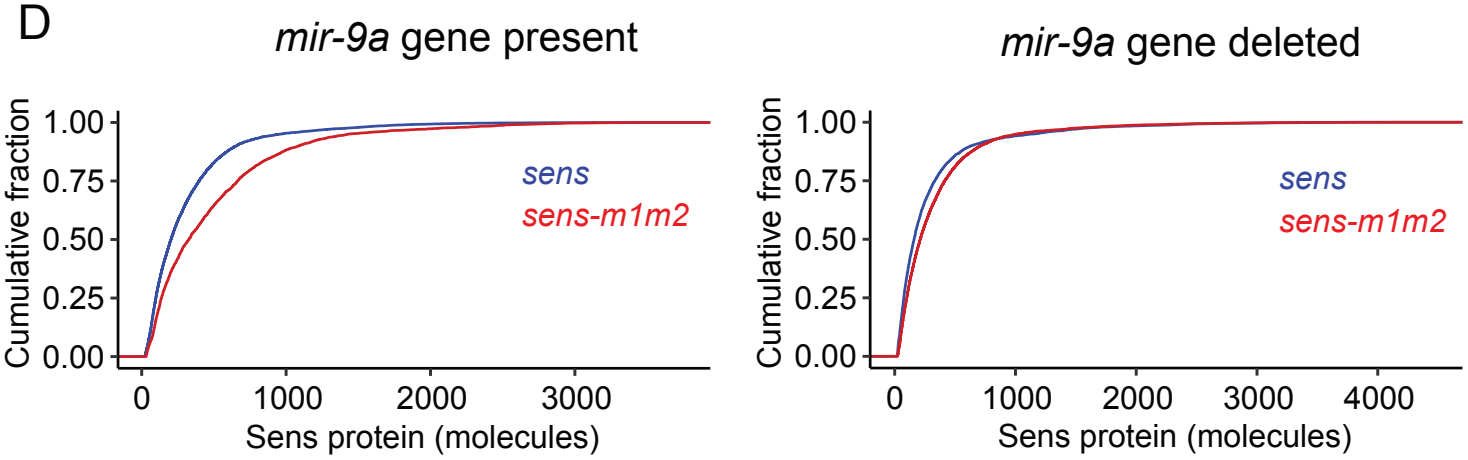

Figure 5

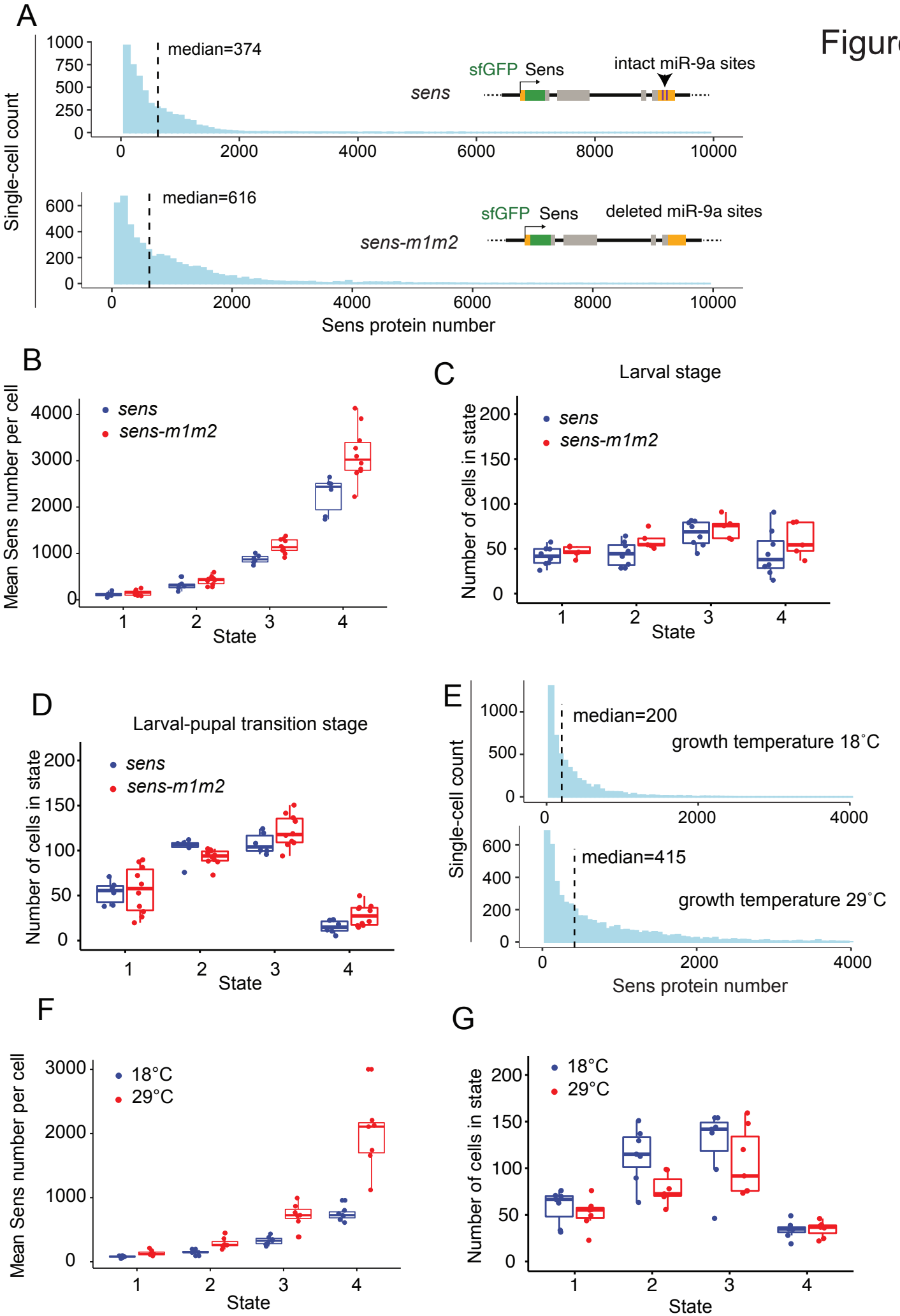
A
Single-cell count
median=374
sens
sfGFP Sens
intact miR-9a sites
median=616
sens-m1m2
sfGFP Sens
deleted miR-9a sites
Sens protein number
B
Mean Sens number per cell
sens
sens-m1m2
State
C
Larval stage
Number of cells in state
sens
sens-m1m2
State
D
Larval-pupal transition stage
Number of cells in state
sens
sens-m1m2
State
E
Single-cell count
median=200
growth temperature 18˚C
median=415
growth temperature 29˚C
Sens protein number
F
Mean Sens number per cell
18°C
29°C
State
G
Number of cells in state
18°C
29°C
State

Figure S7

A

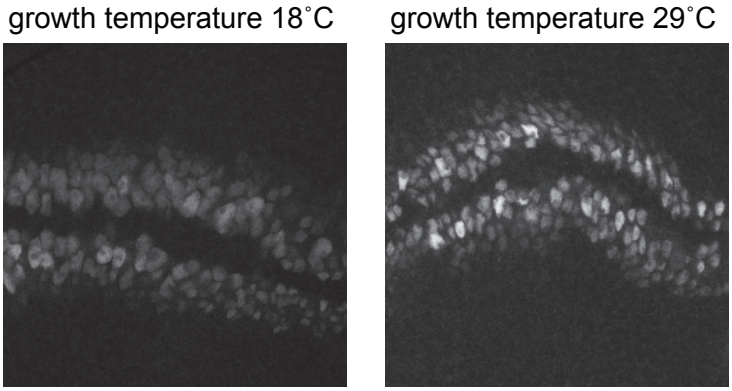

B

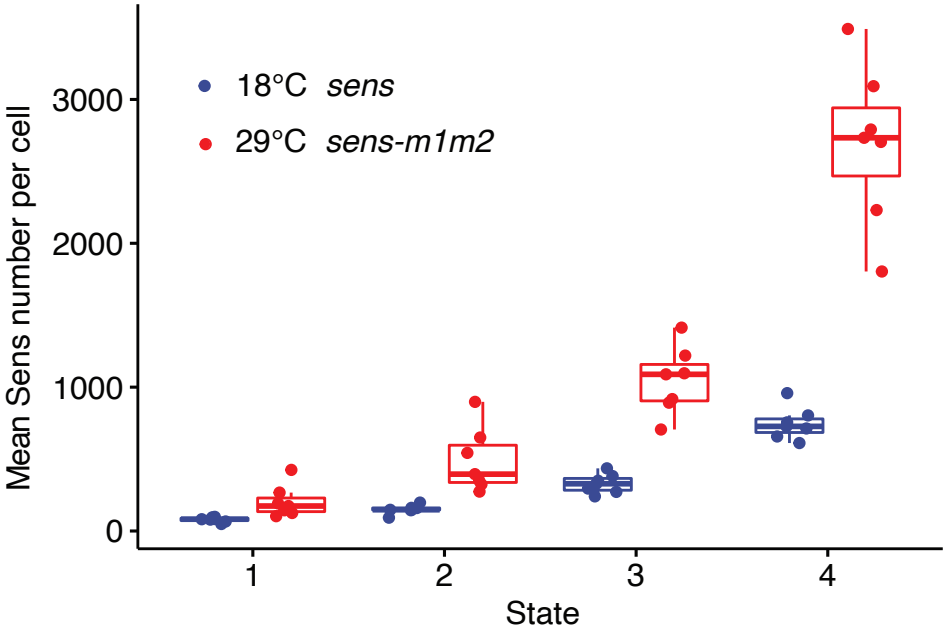

C

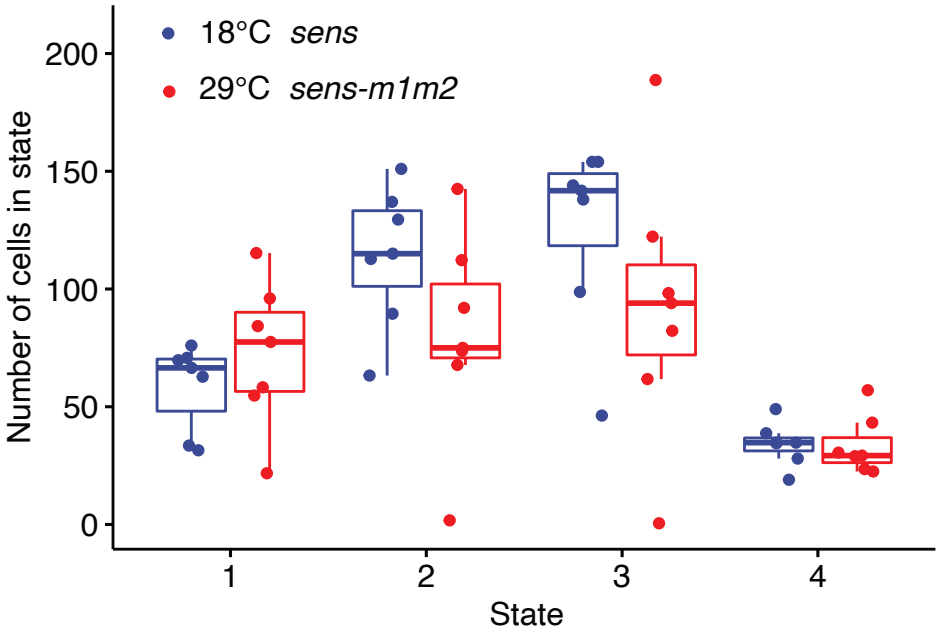

Figure 6

A

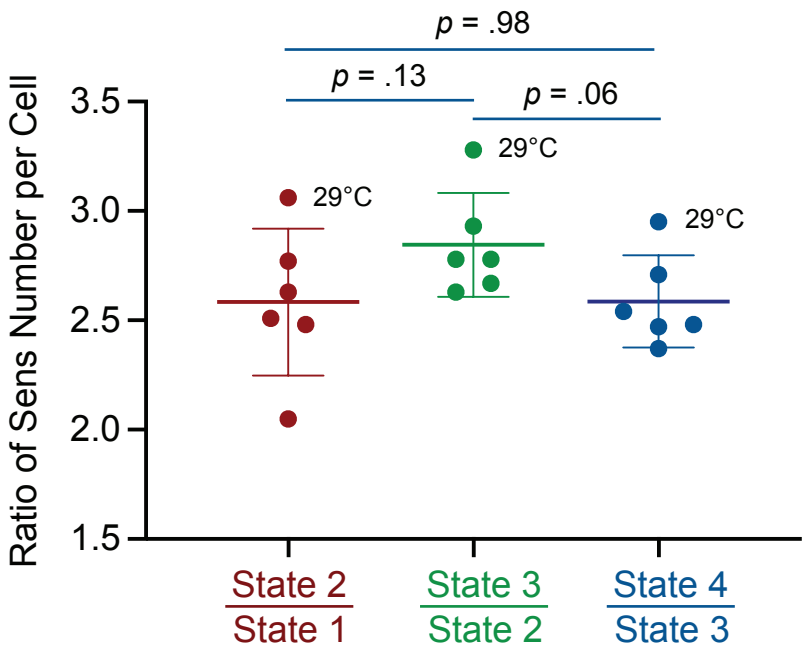
p = .98
p = .13
p = .06
Ratio of Sens Number per Cell
3.5
3.0
2.5
2.0
1.5
29°C
29°C
29°C
State 2
State 1
State 3
State 2
State 4
State 3

B

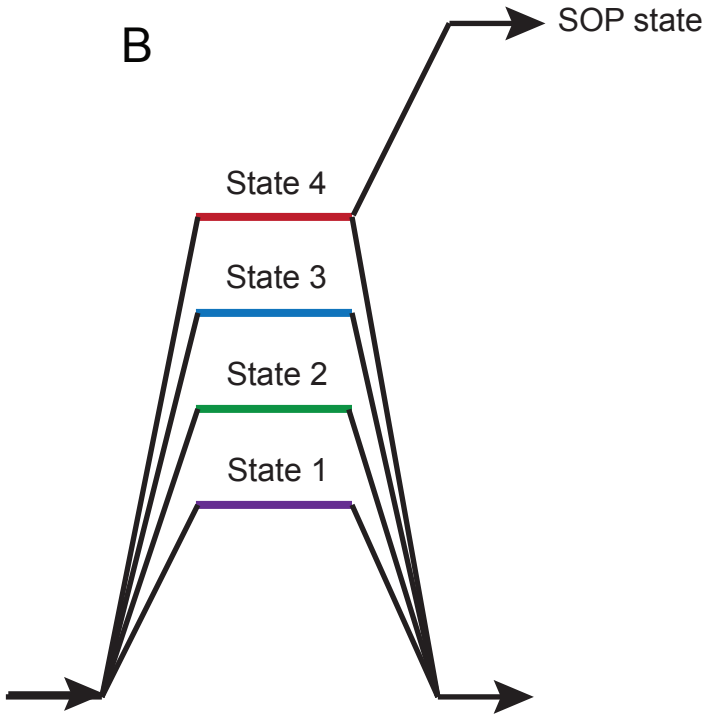
SOP state
State 4
State 3
State 2
State 1

C

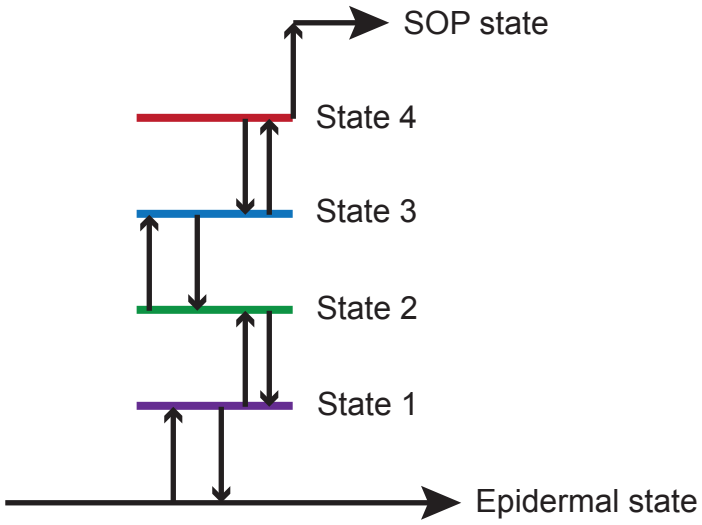
SOP state
State 4
State 3
State 2
State 1
Epidermal state